Master's thesis

NTNU
Norwegian University of Science and Technology
Faculty of Engineering
Department of Geoscience and Petroleum

Kjersti Buraas Snoen

Pre-investigations for High Temperature Borehole Thermal Energy Storage

A part of the future energy solution in Longyearbyen, Svalbard?

Master's thesis in Geotechnology
Supervisor: Randi Kalskin Ramstad
Co-supervisor: Arne Aalberg
June 2021

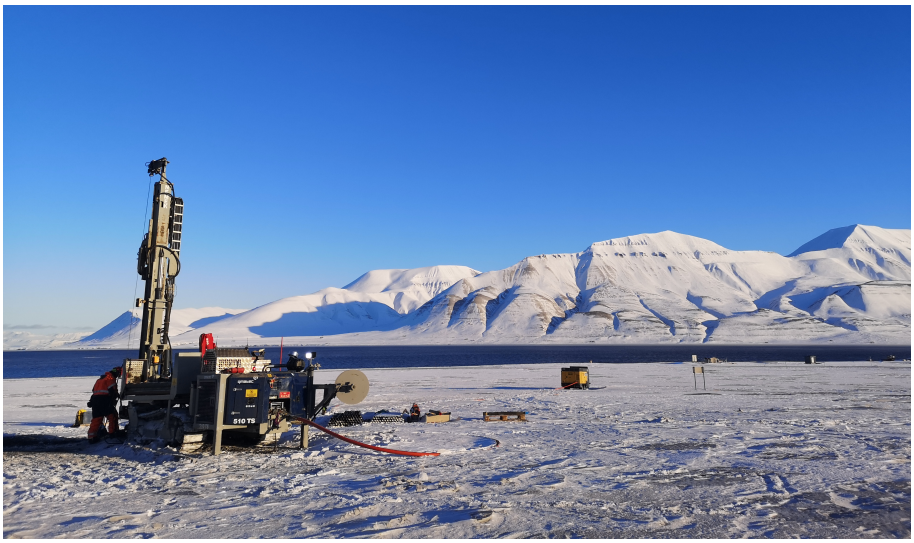

NTNU
Kunnskap for en bedre verden

UNIS
The University Centre in Svalbard

Kjersti Buraas Snoen

Pre-investigations for High Temperature Borehole Thermal Energy Storage

A part of the future energy solution in Longyearbyen, Svalbard?

Master's thesis in Geotechnology
Supervisor: Randi Kalskin Ramstad
Co-supervisor: Arne Aalberg
June 2021

Norwegian University of Science and Technology
Faculty of Engineering
Department of Geoscience and Petroleum

NTNU
Norwegian University of
Science and Technology

NTNU
Norges teknisk-naturvitenskapelige universitet

Fakultet for ingeniørvitenskap og teknologi

Institutt for geovitenskap og petroleum

MASTEROPPGAVE VÅREN 2021

Kjersti Buraas Snoen

Pre-investigations for High Temperature Borehole Thermal Energy Storage

A part of the future energy solution in Longyearbyen, Svalbard?

Bakgrunn

Oppgaven inngår en forundersøkelse med testboring av en energibrønn og termisk responstest med fiberoptiske temperaturmålinger. Hensikten med undersøkelsene er å se på mulighetene for å etablere et storskala borehullsbasert sesongvarmelager i Longyearbyen. Masteroppgaven er gjort i samarbeid med Longyearbyen Lokalstyre som har fått prosjektmidler fra Svalbards miljøfond. Arbeidet er et samarbeid med Lokalstyret, UNIS og Asplan Viak. I en framtidig energiløsning for Longyearbyen med fornybare energikilder som sol og vind, vil sesongvarmelagring være en viktig del.

Oppgave

Oppgaven skal inneholde relevant litteratur om undersøkelsesmetodene og beskrive lab- og feltarbeidet, inkludert presentasjon av resultatene som grunnlag for diskusjon og konklusjon.

Det foreslås følgende innhold i oppgaven:

- Litteraturstudium om termisk responstesting, middels-høytemperatur borehullsbasert sesongvarmelager, distribuerte temperaturprofilmålinger (DTS). Videre om varmeutveksling i grunnen, spesielle grunnforhold i arktiske strøk og røntgendiffraksjon (XRD) for mineralidentifikasjon.
- Beskrivelse av undersøkelsesmetodikk og analysemetoder.
- Systematisere og selvstendig analysere data som blir tilgjengelig fra undersøkelser. Herunder:
    - Erfaringer gjort under boring av testbrønner, samt prøveinnsamling av borekaks.
    - Enkel beskrivelse av innhentet prøvemateriale under boring.
    - Mineralidentifikasjon, XRD, av et utvalg av prøvematerialet innhentet under boring.
    - Analyse av konvensjonell termisk responstest.
    - Fremstilling og analyse av den distribuerte temperaturresponsen i dypet ved bruk av fiberoptiske temperaturmålinger.
- Gjennomføring av feltarbeid i Longyearbyen, inkludert planlegging og etterarbeid inngår i oppgaven. Feltarbeidet gjennomføres vinteren 2021.
- Utføre laboratorieundersøkelser for mineralidentifikasjon, XRD-analyser.
- Utvikle en enkel numerisk modell for sammenligning av resultater fra feltundersøkelser.

Rapporten
Oppgaven skal skrives som en teknisk rapport og ha gode figurer, tabeller og foto. Det skal være fokus på god lesbarhet. Rapporten skal inneholde tittelside, forord, oppgavetekst, sammendrag, innholdsfortegnelse, et fornuftig antall kapitler (med underkapitler), konklusjoner som siste kapittel, referanseliste og vedlegg.

Oppgaven innleveres gjennom Inspera.

Omslag kan med fordel ha en illustrasjon fra oppgaven på framsiden.

Faglærere ønsker en trykket versjon av oppgaven. Faglærer ønsker videre at det lages en pakke med filer fra arbeidet, med rapporten, evt. forsøksresultater, bilder, bakgrunnslitteraturen, elementmodellene, etc. Dette for å lette oppstarten av studentoppgaver som kan tenkes å skulle fortsette undersøkelser på området.

Masteroppgaven skal leveres 10. juni 2021

Trondheim, 7. juni 2021
Randi Kalskin Ramstad, Førsteamanuensis

Abstract

The Norwegian government has decided that today's coal-based energy solution in Longyearbyen, Svalbard is to be changed to a safer and more climate friendly energy solution. A potential solution based on renewable energy sources requires a technology for storing access energy to be retrieved upon need. Borehole Thermal Energy Storage (BTES) uses the underground as a storage medium for thermal energy through an arrangement of boreholes. Knowledge of the material properties is crucial for an efficient BTES design. Thermal Response Test (TRT) is an established field investigation method for determining the ground thermal properties on-site. Fluid with a known added heating effect is circulated in a full-scale borehole, and the thermal response over time is measured. Depth-resolved temperature measurements based on Distributed Temperature Sensing (DTS) technique with optical fiber cables give additional valuable information about the distributed response caused by geological heterogeneity.

Field investigations have been performed to evaluate the possibility of a large scale High Temperature Borehole Thermal Energy Storage (HT-BTES) in Longyearbyen, Svalbard. The field investigation includes test drilling of an energy well and Distributed Thermal Response Test with fiber optic temperature measurements analysed with the infinite line source model. Additionally, drill cuttings samples have been analysed for mineral identification by X-Ray Diffraction, and a 2D numerical model has been made to simulate the thermal response test as a basis for comparison of different methods. The project was initiated by the local government, Longyearbyen Lokalstyre, which has received funding from Svalbards Miljøvernfond. The work was done in collaboration with Longyearbyen Lokalstyre, Asplan Viak, the University Centre in Svalbard (UNIS) and the Norwegian University of Science and Technology (NTNU).

A 198m deep energy well was successfully drilled. The geology encountered is in line with described literature with lithologies of shale, siltstone, and sandstone of the Carolinefjellet Formation and the underlying Helvetiafjellet Formation. The groundwater level was assumed to be at 40m depth, and filled from below by an overpressured aquifer in the Helvetiafjellet Formation. The mean value of the estimated distributed ground thermal conductivity agrees with the calculated value of 3.4W/(m,K) from the conventional TRT. The distributed estimate shows that the most significant heat transfer occurs down flow in the upper part of the water-filled part of the borehole. The heat transfer in the lower part of the borehole is viable with a correlation between the thermal conductivity of depth sections and fluctuations in the quartz content through the stratigraphy. A borehole thermal resistance of 0.06-0.1(m,K)/W was estimated depending on the value of undisturbed ground temperature used. The numerical model gives an outer boundary at 1.75m radius for the expected extent of the surrounding ground being affected by the TRT. The pre-investigation results are promising for a potential HT-BTES system in Longyearbyen, and it is recommended to proceed with further investigations. Suggested improvements of the performed field investigations include manual measurements of the groundwater level, taking water samples during drilling to compare with known groundwater aquifers in the area, extend the time period for depth-resolved temperature measurements during the recovery period and calibrate a section of the optical fiber with a known temperature and time record in the field.

Sammendrag

Den norske regjeringen har besluttet at det kulldrevne energiverket i Longyearbyen, Svalbard skal stenges ned og erstattes av en sikrere og mer klimavennlig energiløsning. En potensiell løsning basert på fornybare energikilder krever at det finnes teknologi for lagring av overflødig energi som kan hentes ut i perioder med større behov. I et borehullsbasert termisk energilager lagres termisk energi i undergrunnen ved hjelp av et oppsett av borehull. Et effektiv design av et borehullsbasert termisk energilager er i stor grad avhengig god kunnskap om materialegenskapene i lagrinsvolumet. Termisk Respons Test (TRT) er en veletablert feltundersøkelses-metode for bestemmelse av den stedspesifikke undergrunnens termiske egenskaper. Et fluid med en kjent tilført varmeefffekt sirkuleres i et fullskala borehull, og temperatur-responsen måles over tid. Temperaturmålinger i dypet basert på distribuerte temperaturmålinger (DTS) med optiske fiberkabler gir tilleggsinformasjon om den distribuerte responsen i dypet som følge av geologiske heterogeniteter.

Feltundersøkelser er blitt gjennomført for å evaluere om et potensielt storskala høy-temperatur borehullsbasert termisk energilager i Longyearbyen, Svalbard er mulig. Feltundersøkelsene inkluderer boring av en fullstendig energibrønn og gjennomføring av en termisk respons test med distribuerte temperaturmålinger. I tillegg er prøver av borekaks blitt samlet inn under boring og analysert for mineralsammensetning, og en enkel 2D numerisk modell har blitt utviklet som sammenligningsgrunnlag for resultatene fra feltundersøkelsene. Prosjektet er iverksatt av Longyearbyen Lokalstyre som har mottatt prosjektstøtte fra Svalbards Miljøvernfond. Prosjektet er utført som et samarbeid mellom Longyearbyen Lokalstyre, Asplan Viak, Universitetssenteret på Svalbard (UNIS) og Norges teknisk-naturvitenskapelige universitet (NTNU).

En 198m dyp energibrønn ble suksessfullt boret. Den påtrufne geologien samsvarer med det som er skrevet i litteraturen for området. Litologiene består av skifer, siltstein og sandstein fra Carolinefjellet Formasjonen og den underliggende Helvetiafjellet Formasjonen. Energibrønnen ble naturlig fylt med grunnvann, trolig fra en artesisk akvifer i Helvetiafjellet Formasjonen. Under testing lå grunnvannsnivået på omlag 40m dyp. Gjennomsnittsverdien av de estimerte verdiene for konduktivitet av de distribuerte seksjonene i dypet samsvarer med den utregnede verdien på 3.4W/(m,K) fra den konvensjonelle TRT. De distribuerte temperaturmålingene viser at den største varmeoverføringen skjer i de øvre delene av den vannfylte delen av borehullet i kollektorkanalen med nedadgående strømning. Varmeoverføringen i den nedre delen av borehullet kan korreleres til fluktuasjoner i kvartsinnholdet gjennom stratigrafien. Uforstyrra temperatur i grunnen gir grunnlag for å estimat av borehullsmotstanden som er estimert til 0.06-0.1(m,K)/W. Den numeriske modellen gir en ytre grense for den forventende omkretsen av omsluttende berggrunn som påvirkes av testen tilsvarende en radius på 1.75m. Resultatene av forundersøkelsene er lovende for et potensielt storskala høy-temperatur borehullsbasert termisk energilager i Longyearbyen. Feltundersøkelsene kan forbedres ved å inkludere manuelle målinger av grunnvannsnivået, samle vannprøver under boring som kan sammenlignes med kjente grunnvannsakviferer i området, tiden for målinger i perioden etter test-slutt anbefales at utvides samt at en seksjon av fiberen kalibreres med en kjent temperatur og tids-sekvens ute i felt.

Contents

Cover picture: Drilling at Hotellneset, Longyearbyen (Svalbard). Photo: Kjersti Buraas Snoen.

Preface

This master thesis is a part of a project initiated by the local government in Longyearbyen, represented by the project leader Rasmus Bøckman. The project is a collaboration with Longyearbyen Lokalstyre, the consultant company Asplan Viak, the University Center in Svalbard (UNIS), and the Norwegian University of Science and Technology (NTNU). Asplan Viak has organized the work and provided equipment and data for the conventional Thermal Response Test. A report of the pre-investigations are independently prepared by Asplan Viak. The thesis has been developed under guidance from main supervisor Randi Kalskin Ramstad and co-supervisor Arne Aalberg. This master thesis gives an additional contribution to the project with results from observations of the drilling process, sampling and preparation of drill cuttings samples for mineral identification analysis, analysis of depth-resolved temperature measurements and a 2D numerical model for comparison with results from field investigations. Taking part in planning, operational tasks during and after fieldwork has been a significant part of the work in addition to presenting the results in this report. Two additional students are connected to the project, namely: Marko Piitu Eemeli and Lars Mogstad. Their thesis includes work on laboratory testing of thermal properties of rock piece samples and numerical modelling of a potential storage system.

I strongly believe there is a lot of experience and knowledge to gain from being out in the field, asking questions, and solving challenges that arise along the way. And challenges surely arise when operating in the high Arctic, but with experienced and motivated people around you - everything sorts out in the end. The days in the field would not have been the same without fellow student Piitu Kurtila helping out and bringing insights to the discussions, and to the drill operators Trond and Lars from LNS and Øslandet Brønn og Energiboring - thank your for sharing your much appreciated knowledge and good laughs out in the field. I am much grateful for the opportunity to be present and taking action in all involved processes during the fieldwork. For this, I would like to thank UNIS for hosting me as a guest master student, the staff at the Logistics Department for technical support, necessary training and equipment in the field, and associate professor Aleksey Shestov for helping out with organizing my stay at UNIS. The financial support for my stay was provided by The Norwegian Tunneling Society (NFF), for which I am very grateful.

Additionally, I would also like to acknowledge the use of the lab facilities and help from Torill Sørløkk and Laurentius Tijhuis at the Chemical Mineralogical Laboratory. And to my supervisors for always being available for discussion and bringing insight to the work.

Kjersti Buraas Snoen
Trondheim, June 2021

Introduction

The Norwegian government presented at the beginning of the year that the coal-based power plant in Longyearbyen is to be changed to a safer and more climate friendly energy solution within the next few years (Press release nr 003/2021). Longyearbyen is located at 78° north on the central Spitsbergen (Figure 1), and serves as the administration center at the archipelago Svalbard. The foundation and development of the city are based upon coal mining (Reymert 2013). Several options for a new energy solution has been investigated and presented (Tennbakk et al. 2018), after order from the Norwegian Ministry of Petroleum and Energy. The long distance and transport overseas favors local energy sources. The work on renewable energy solutions based on solar energy and wind has evolved over the recent years, and the potential at Svalbard has shown to be good. Nevertheless, the strong difference in seasons and remote location rises the need for storing access energy to be retrieved upon need. Could a Borehole Thermal Energy Storage (BTES) be feasible as a part of the future energy solution for the remote northern community of Longyearbyen?

A Borehole Thermal Energy Storage (BTES) system can store thermal energy on a large scale over seasons, utilizing the volume of the ground to store the thermal energy through an arrangement of Borehole Heat Exchangers (BHE). As the technology for renewable energy sources and production develops, BTES technology for energy storage is an interesting piece in the puzzle towards a future based on green energy. Climate change has been a topic of large public interest over the last years. The Arctic area hits the top of the hot discussion having future climate scenarios predicting a warmer and wetter environment, happening at increased speed compared to the rest of the world (Adakudlu et al. 2019, Isaksen et al. 2017, AMAP 2017).

A successful design of a BTES system are strongly related to proper pre-investigations studying the specific material properties on site. Thermal Response Test is a broadly used field investigation method used to determine the effective ground thermal conductivity and borehole thermal resistance. This master thesis is part of a project initiated by the local government in Longyearbyen, Longyearbyen Lokalstyre, and funded by Svalbards Miljøvernfond. The purpose of the project has been to perform pre-investigational studies in Longyearbyen to determine if a High Temperature Borehole Thermal Energy Storage is feasible. The project has been a collaboration between Longyearbyen Lokalstyre, the consultant company Asplan Viak, the University Centre in Svalbard (UNIS), and the Norwegian University of Science and Technology (NTNU). The project has received interest from the media found

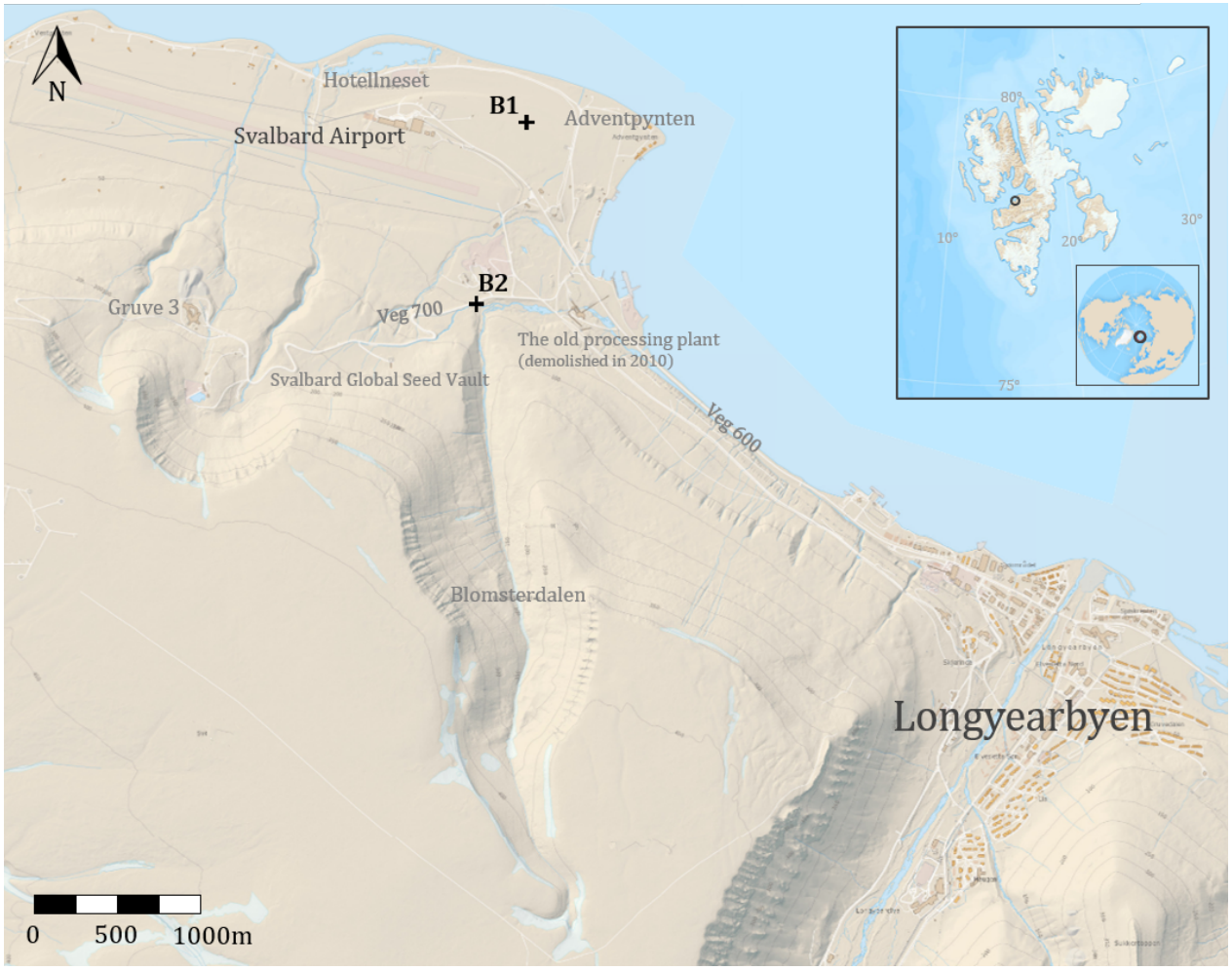

Figure 1: Map of Longyearbyen and Svalbard, modified from TopoSvalbard (Norsk Polarinstitutt n.d.*a*).

in High North News (Ylvisåker 2021) and Teknisk Ukeblad (Viseth 2021).

The master thesis aims to firstly give a literature review of seasonal underground thermal energy storage systems, factors influencing the ground thermal properties, and in-situ field investigations by Thermal Response Test and temperature measurements based on Distributed Temperature Sensing technique. The field site is described in Chapter 2, followed by the methodology of the field investigations and data analysis. The results are given in Chapter 3, accordingly discussed and concluded. The work on the thesis resulting in this report has included observing the drilling process and collecting drill cuttings samples, taking part in the operational tasks during the Thermal Response test including depth-resolved temperature measurements, preparing a selection of the drill cutting samples for X-ray diffraction analysis, analysing the conventional TRT data based on a template provided by Asplan Viak, independently find a solution to systematize and analyse the obtained data from the depth-resolved temperature measurements with optical fiber and producing a simple 2D numerical model to compare with results from the field investigations.

1 Literature review

1.1 Seasonal underground thermal energy storage

The underground provides large volumes of space that may be used as a storage medium for large quantities of thermal energy to be stored over short- and long-term periods, vaguely defined as seasonal and/or underground thermal energy storage. This is a general definition and different systems are further defined based on the classification of the underground material, operating temperature, system size, and application (Gehlin 2016). The following section is based on Gehlin (2016) unless other is specified.

Borehole Thermal Energy Storage (BTES) system utilizes boreholes perforating the underground to transfer heat from the boreholes to the surrounding ground for storing, see Figure 1.1. Heat carrier fluids circulating inside the borehole generate the heat exchange with the surrounding underground, referred to as Borehole Heat Exchangers (BHE). A collector pipe is commonly installed inside the borehole, but open systems where the heat carrier fluid is in direct contact with the surrounding ground also exist.

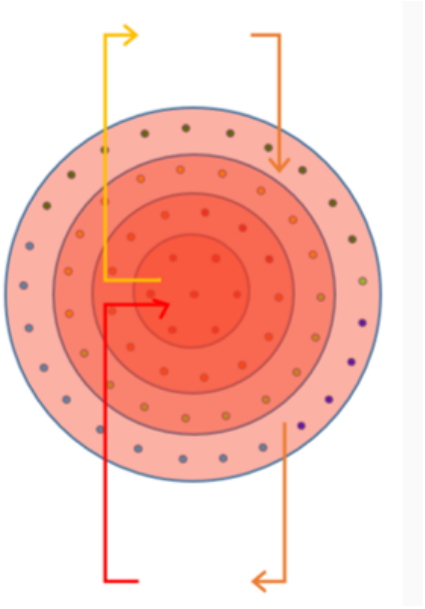

Figure 1.1: Conceptual presentation of a Borehole Thermal Energy Storage. The arrows represents heat being added and extracted. Different temperature in the storage region is presented by the red temperature gradient. The small circles represents boreholes. Figure provided by Asplan Viak.

The storing capacity is a function of the storage volume and the ground material capacity to store and conduct heat. High volumetric heat capacity and thermal conductivity are therefore desirable, these terms are further described in subsection 1.2.1. Heat transfer occurs mainly by conduction, thus high thermal conductivity assures effective heat transport. Consequently, high thermal conductivity also increases the heat loss from the store. The ground thermal conductivity is normally in the range of 1-5 W/(m·K). Water saturation, high bulk density, and quartz content are typical for the formations with higher thermal conductivity values. In addition to the material properties of the storage volume, the properties of the BHS must also be

taken into account. This is referred to as borehole thermal resistance, as an expression for the difference in temperature between the heat carrier fluid and the surrounding ground. To assure good thermal contact between the fluid channels in the borehole and the surrounding ground, the borehole may be grouted or groundwater filled. Where the latter one is most common in Scandinavia.

It is commonly assumed that the mechanism of heat transfer is mainly by conduction. The presence of groundwater on the other hand complicates those assumptions, adding the mechanism of convective heat transfer. Where the convective flow can be induced by the regional groundwater flow in the located area, or thermally induced natural convection due to temperature gradients when exerting the BHE for heat injection or extraction (also called thermosiphon effect). Although Nordell (1993) argues for the contribution to be so small that it can be neglected, Gehlin (2002) gives an example of a rock with thermal conductivity of 3.5 $W/(mK)$ and a model of fracture groundwater flow that showed an increase in effective thermal conductivity by 6% to 3.7 $W/(mK)$ with the convective heat transfer contribution compared to the purely conductive cause - although the contribution seems small the total effect may by significant for a large system.

Where the BTES system's storage capacity is proportional to its storage volume, the heat losses are proportional to its surface area. Increasing the storage volume decreases the relative heat loss. Hence, an effective design involves compact geometry and large storage volume, i.e., small surface to volume ratio. For this reason, the BTES technology is the most efficient for heat storage at large scale. Additionally, Hellström (1991) proposes to cover the surface area above the storage region with a shallow layer of soil with low thermal conductivity as a possibility to reduce the heat loss from the storage region.

BTES systems have a great potential of increasing the efficiency of energy systems by its potential to store excess energy for later use, making a more sustainable energy system. Introducing a BTES system may reduce the emissions of greenhouse gases and air polluting gases if the BTES facilitate for increased energy utilization and replacement of fossil energy sources. In addition, a BTES system is areal effective and unobtrusive at the surface, quiet and requires little operational and maintenance costs. The concept of storing energy gives the opportunity to control changes in energy demand, especially applicable for areas with strong differences in seasonal climate (Skarphagen et al. 2019). A BTES system can balance the need for cooling in the summer by storing excess heat which thereafter can be extracted during winter.

According to Nordell (1993) the first idea of storing heat in borehole heat stores arises in the middle of 1960s with the idea of injecting high temperature steam into boreholes of rocks, the idea was further developed and modified in Sweden with the Sunstore project in 1977. Several borehole pilot plants were made in the following years, alongside with theoretical work which consequently led to mathematical modelling of borehole heat stores. The first large scale borehole heat store was constructed in 1982 at Luleå University of Technology, and in operation the year after.

1.1.1 High Temperature Borehole Thermal Energy Storage (HT-BTES)

BTES systems can be categorized based on the temperature in the storage region; low and high temperature BTES. Where the low temperature storage system has temperatures in the region close to the undisturbed ground temperature. High temperature systems are typically large-scale systems appropriate for district heating networks and industrial processes based on solar or waste heat. Temperatures are typically in the range above 30°C, leaving the need for heat pumps because of the temperature gradient. For systems operating above 60°C, special care should be made regarding material use and environment. For systems ranging above 100°C, technical issues regarding boiling groundwater, material properties, and environmental aspects must be taken into account.

1.1.2 BTES in an Arctic environment

Giordano & Raymond (2019) accentuate the challenges of the development of renewable energy technologies in the Arctic. The locations are typically remote with extremely cold temperatures that gives technical barriers. Additionally, it is pointed out that the storage issues due to the gap in energy supply and demand are more compelling than in temperature climates. A first design of BTES in a subartic climate was made, indicating the technology of underground storage to be viable in a subarctic climate. The study site was located in discontinuous scattered permafrost, but free of frozen ground due to a talik around a nearby lake.

1.2 Ground thermal properties

1.2.1 Heat transfer

Heat is the thermal energy moving from one system to another system of lower temperature, this is governed by nature by conservation of energy and establishing equilibrium. The mechanism of heat transfer is based upon the principles:

- Conduction - heat is transferred by contact from molecule to molecule.
- Convection - heat transfer due to fluid motion induced by density gradients.
- Radiation - heat transfer due to electromagnetic waves.

The thermal properties of a material can be described in terms of:

- Thermal conductivity (λ) - the ability to conduct heat $[W/(m,K)]$.
- Heat capacity (C) - the amount of energy needed to raise the temperature by one unit degree $[J/K]$.
- The specific heat capacity (c_p) - the heat capacity per unit mass of a material $[J/kg,K]$.
- Thermal diffusivity (a) - the rate of which heat is transferred $[m^2/s]$.

Which can be expressed by the relationship:

$$a = \frac{\lambda}{\rho c_p} = \frac{\lambda}{c_V} \qquad [m^2/s] \tag{1.1}$$

Where ρ is the density of the material $[kg/m^3]$, which together with the specific heat capacity (c_p) expresses the volumetric heat capacity (c_V) $[J/(m^3, K)]$.

Hellström (1991) gives typical values for sedimentary rocks in Sweden after age, the values are calculated based on assumed porosity and mineral content, see Table 1.1.

Table 1.1: Thermal properties of sedimentary rocks of Mesozoic age, based on Swedish investigation (Hellström 1991).

Rock type	λ **[W/(m,K)]**	c_p **[J/(kg,K)]**
Sandstone (Mesozoic)	2.3-4.5	2000-950
Shale (Mesozoic)	1.5-3.0	2200-1100

1.2.2 Subsurface temperatures

The temperature of the ground is a result of several processes and factors: initial conditions and loading conditions, thermal and hydraulic properties of the ground, and the surface boundary conditions (Nordell 1993).

The thermal properties of the solid material, i.e., rock or soil components of the underground volume, are highly dependent on the mineral composition and orientation (Nordell 1993, Andersland & Ladanyi 1994). Nordell (1993) accentuate that classification of a rock type allows for a relative large variation in mineral composition, so that the most accurate values are obtained from laboratory testing of representative samples. Andersland & Ladanyi (1994) points out the amount of quartz in the mineral composition as an important factor, as quartz has a very high thermal conductivity.

The total heat flux and boundary conditions at the ground surface are rather complex (Figure 1.2, left). The physical processes include shortwave and longwave radiation, convective and conductive heat flow, evaporation, and condensation. Where the amount of solar shortwave radiation added to the heat flux is highly dependent on the surface ability to absorb/reflect the incoming radiation together with cloud cover, latitude and atmospheric conditions. The net longwave radiation from the ground depends on surface and air temperature, vapor pressure, and cloud cover, but is assumed relatively constant over time. The convective heat flow depends on factors such as the difference in air and surface temperature, wind velocity, and surface roughness causing air turbulence. In the

case of still air and the ground being colder than the air - the air close to the grounds gets colder and the air profile remains stable as the most dense air interacts with the ground surface, and the heat transfer occurs mainly by conduction. Having the ground warmer than the air will cause the air at the ground surface to heat and rise, creating a conductive current. Heat fluxes from evaporation and condensation depend on vegetation and soil moisture content. As a complete analysis of the physical processes involved in the total heat flux $[W/m^2]$ at the ground surface are complex and can be difficult to achieve, indexes of freezing and thawing based on air temperature together with surface factors are often used (Andersland & Ladanyi 1994).

Seasonal and daily changes in air temperature cause cyclic variations in the ground temperature, with decreasing amplitude with increasing depth (Figure 1.2, right). At a certain depth, the annual temperature variation is negligible and approximate constant over the year, also described as the mean annual temperature. The temperature may further be described linearly with increasing temperature at increasing depth due to the effect of the geothermal gradient (heat flow from the earth interior). As mentioned above, the analysis of air temperature can be used together with empirical surface factors to compensate for the influence of net radiation, vegetation, insulating snow cover, surface relief, drainage, thermal properties of the ground etc. Note that the surface factor is often different for thawing and freezing (Andersland & Ladanyi 1994).

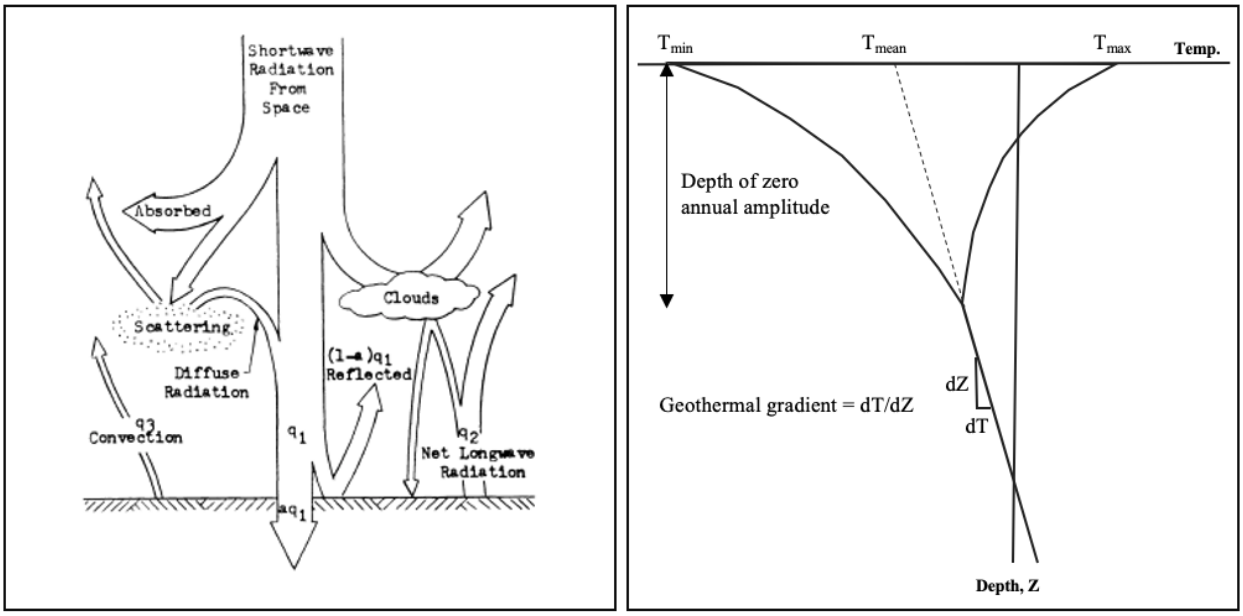

Figure 1.2: Left: Heat transfer at the ground surface. Heat flux contribution from short wave radiation (q_1) (with a being the ground absorptivity), net long-wave radiation (q_2), convective heat flow to the air (q_3) (Andersland & Ladanyi 1994). Right: A graphic presentation of the cyclic air temperatures affecting the ground temperature and the influence of the geothermal gradient, modified after Andersland & Ladanyi (1994).

The convective heat transfer in the underground volume is highly dependent on the hydraulic properties of the ground. The convective heat flow may be caused by geohydrological conditions, i.e., regional groundwater flow (forced convection) or thermally induced natural convection due to the difference in temperature between the BHE and the surrounding ground (buoyancy effects). The hydraulic conductivity gives a number on how a specific

fluid can flow in a geological material, including the permeability of the material, density, and viscosity of the fluid. In bedrock, the hydraulic conductivity is highly dependent on the fractures and the aperture of the fractures. The hydraulic conductivity together with the local groundwater gradient gives the magnitude of the groundwater flow (Nordell 1993).

The initial conditions will be the ground equilibrium state as a sum of all these mentioned processes, when no loading condition is exerted.

1.2.3 Frozen ground

The following subsection on frozen ground is based on Andersland & Ladanyi (1994) if nothing else is specified.

Perennially frozen ground, permafrost, is defined as ground with temperature below 0°C for a minimum of two consecutive years. This can be in both bedrock and soil, with and without the presence of moisture (water and ice). The top layer of the ground exerted by thawing and freezing over the seasons are referred to as the active layer. The thickness of the active layer varies, dependent on the local ground properties and the amount of heat extracted during winter/ entered during summer.

Areas with permafrost can be divided into different zones dependent on the spatial distribution and temperature. The International Permafrost Association (2021) classifies continuous permafrost as areas where 90-100% of the landscape underlies permafrost, discontinuous permafrost in areas with 50-90% and sporadic permafrost where 0-50% underlies permafrost. Andersland & Ladanyi (1994) use the -5°C isotherm of the mean annual ground temperature as criteria to divide between zones with continuous and discontinuous permafrost.

Water bodies have a significant influence on the thermal regime in a permafrost area. Lakes with unfrozen water during winter will warm the basin underneath. At a lake diameter exceeding the permafrost thickness, the unfrozen zone beneath will extend through the permafrost thickness. The effect is not as presiding under lakes which completely freeze during winter, but there are still some reductions in permafrost thickness due to the efficient thawing of the lake compared to the surrounding ground. Rivers can be treated as small lakes, and the ocean as a deep lake in terms of its thermal effect. A layer or body of unfrozen ground enclosed by permafrost is referred to as a talik, further divided into closed or open whether the surrounding permafrost is enclosed entirely or partially.

Frozen ground is a multiple phase system consisting of solid particles (minerals and ice), liquid water, and gas. Andersland & Ladanyi (1994) treat it as a four-phase system defining ice as a respective phase, see Figure 1.3. The presence of ice in frozen ground can have several forms, from simply covering single mineral particles to ice lenses and massive ice deposits. Frozen ground can contain unfrozen water as thin films on the surface of particles (bonded water) or due to salts in the pore water. Dissolved salts in the pore water lowers the freezing temperature, i.e., increases the freezing point depression (ΔT below 0°C) and increases the unfrozen water content. Salt ions do not fit in the crystal lattice of ice. As water freezes, this consequently leads to a pore brine solution with increasing salt ions.

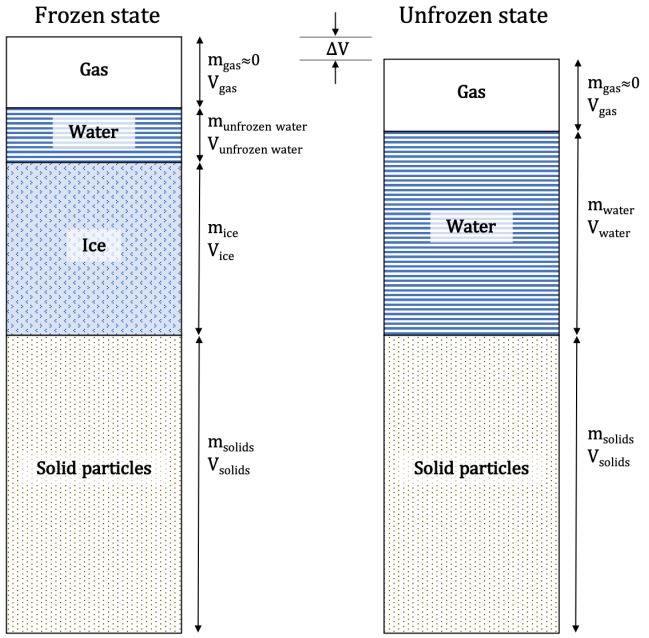

Figure 1.3: Multiple phase system of frozen ground, modified after Andersland & Ladanyi (1994).

Latent heat of fusion is the heat energy absorbed or released during a phase change between solid and liquid. The latent heat of fusion for H_2O at 0°C is 333.7 kJ/kg. Thus, per unit mass of ice melting to water, 333.7 kJ is absorbed. And likewise, 333.7 kJ released per unit mass of water freezing into ice without change in temperature. For a ground volume, the total energy involved in the phase change process depends on the ground water content. The ground volumetric heat of fusion (L) can be expressed by the equation:

$$L = \rho_d L' \frac{w - w_u}{100} \tag{1.2}$$

Where L' is the latent heat of fusion for H_2O at 0°C; ρ_d is the dry density of the ground; w is the total water content; and w_u is the unfrozen water content. The latent heat of fusion during the phase change process gives the ground an apparent heat capacity different from the ground heat capacity of the ground constituents alone (mineral solids and water). This must be accounted for when operating in temperatures at and around the ground freezing point.

1.2.4 Mineral identification by X-ray diffraction analysis (XRD)

X-ray Diffraction (XRD) analysis is a nondestructive and fast laboratory method that can be used for mineral identification (Grimstvedt & Korneliussen 2000). The method is based on the crystal lattice diffraction of X-rays. As the incoming X-ray beam interacts with the crystalline material in the sample, the beam gets diffracted by Bragg's law (Equation 1.3, illustrated by Figure 1.4). Detection and processing of the diffracted X-ray beams gives a diffraction X-ray pattern (diffractogram), where the pattern represents the intensity of the X-ray beam as a function of the double Bragg angle 2θ. In a crystal lattice there are several planes set in a specific structure, and the maximum of

each X-ray diffraction pattern correlates with a distinct interplanar spacing (Kovalev et al. 2017). The method requires that there are calibrated samples for interpretation of the results, a database of known crystalline structures. For powder samples, accuracy in the sample preparation is pointed out as an important factor for achieving good results (Grimstvedt & Korneliussen 2000).

$$n\lambda = 2dsin\theta \tag{1.3}$$

Where n i the order of diffraction (a whole number integer), λ is the wavelength of the incident radiation. d is the distance between parallel planes of atoms in a crystal lattice and θ is the diffraction angle. With a fixed X-ray wavelength (λ), a diffraction peak is produced by a set of planes only at a specific angle (θ). Hence, the peak positions are determined by the space between the diffracting planes of atoms (d), and the peak intensity by what atoms are in the diffracting plane.

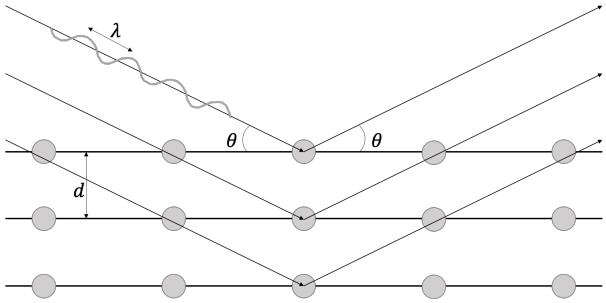

Figure 1.4: Bragg diffraction of X-rays with wavelength (λ) at a diffraction angle (θ) in a crystalline material with an interplanar distance (d) between the parallel atom planes.

1.3 In situ field investigation, Distributed Thermal Response Testing (DTRT)

The thermal properties of the ground are distinctly related to the geology and ground conditions on site. This favors in situ field measurement for determining the thermal properties, compared to laboratory testing of samples and choosing parameter values from tables. The dimensioning of a BHE installation is largely dependent on the thermal properties of the ground and the borehole thermal resistance, with an increasing degree of crucially the larger the system is (Signorelli et al. 2007). Thermal Response Testing (TRT) is a known and broadly used in situ field measurement technique that gives information about the thermal properties at a specific location, including the influence of groundwater flow, water-filled cracks, fissures and layers within the bedrock etc. The borehole that is used for testing may later be included in the final system design. The principle of a TRT is to exert the ground for a temperature injection at a known load, this will disturb the ground thermal equilibrium. The ground thermal properties and the borehole thermal resistance are then estimated by interpreting the measured response over time (Gehlin 2002). See Figure 1.5 for conceptually set-up of a TRT test with a mobile TRT rig.

According to Gehlin (2002) the first presentation of thermal response test as a method for in situ measurements of the ground thermal properties was done by Mogensen in 1983. This method was based on using a circulating cooling fluid and continuous measurements of the outlet fluid temperature. The thermal response was compared with a mathematical model of the heat transfer process. The method was used to evaluate several existing systems, and further served as a basis for the development of the first mobile measurements devices for thermal response testing. These mobile devices were independently constructed by Eklöf & Gehlin (1996) and Austin III (1998) at Luleå Technical University and Oklahoma State University respectively.

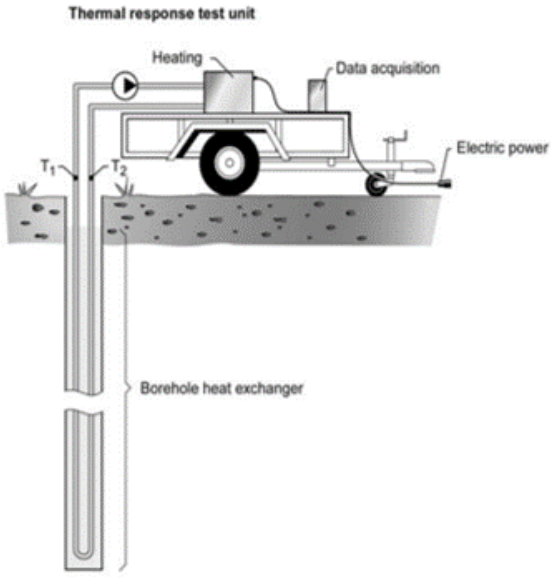

Figure 1.5: Conceptual set-up of Thermal Response Test, from Gehlin (2002).

The conventional TRT set up record temperatures at the pipe inlet and outlet, and the resulting thermal properties of the ground represent an average of the borehole depth. Advanced thermal response test methods combine the conventional set-up with depth-resolved temperature measurements, referred to as Distributed Thermal Response Test (DTRT). The use of DTRT was first proposed and demonstrated by Acuña (2013). The DTRT methods determine the local thermal properties at depth, including the borehole thermal resistance. Acuña (2013) found the local ground thermal conductivity to vary slightly with depth, but that the average agreed well with the results from the conventional TRT. On the other hand, the local borehole thermal resistance was found to be lower than the effective resistance given by the conventional TRT analysis due to overestimation of the fluid temperature. The distributed temperature measurement gives a better tool to distinguish different geological features such as layering, fractured zones, and groundwater flow which consequently may influence the local properties at depth. Hence, the DTRT gives a more detailed and realistic representation of the underground and so better design parameters (Wilke et al. 2020).

In addition to geological heterogeneity that can cause particular layers to dominate the heat transfer, the heat transfer is in reality also influenced by the natural temperature gradient caused by the ground surface. In the case of heat injection, the heat transfer from the fluid to the ground might be highest near the surface and opposite in the case of heat extraction due to the temperature gradient. The ground thermal conductivity estimated from a conventional TRT heat injection test may therefore differ dependent on the BTES system operational mode (Signorelli et al. 2007).

Use of optical fiber cables is the technique most commonly reported in the literature for distributed temperature measurements in a DTRT (Wilke et al. 2020). There are reported different configurations with the optical fiber cable placed both on the inside and outside of the collector pipe. The temperature is recorded as a continuous profile

along the optical fiber cable, based on Distributed Temperature Sensing (DTS)methods. These are optoelectronic devices, i.e. electronic devices sending and detecting light signals. The main principle is based on detection of backscattered light from laser pulses sent into the optical fiber cable (Ukil et al. 2012).

According to Ukil et al. (2012) are optical fiber cables mainly made of material of either glass or plastic, with the latter one typically for applications of very short distances and is consequently let out of the further explanation. Doped quartz glass has the specific crystal structure (lattice) of silica. Lattice oscillations are caused due to thermal effects along the cable. Scattering of the light occurs when light from the laser pulses hits the molecular oscillations due to an interaction between the photons of the light particles and the electrons of the molecule. The backscattered signal contains different spectral components; the temperature-independent Rayleigh scattering with a wavelength equal to the incoming light from the laser source and the temperature-dependent Raman scattering with altered frequency. The Raman scattering has two components; the Stokes-Raman and Anti-Stokes-Raman with higher and lower wavelength than the original light respectively. See Figure 1.6 It is the intensity of the Anti-Stokes-Raman scattering which is temperature dependent, whereas the intensity of the Stokes-Raman scattering is temperature insensitive. The local temperature of the backscattered signal origin can then by measured by the ratio of the two Raman components intensities. The location, i.e. the borehole depth, is acquired by measuring the signal transit time (Wilke et al. 2020).

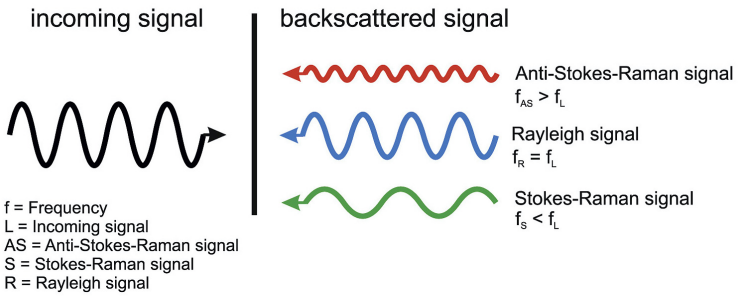

Figure 1.6: The principle of Distributed Temperature Sensing are based on sending a laser pulse (incoming signal) and detection of the backscattered signal with components of different frequencies. From Wilke et al. (2020).

The influence of groundwater flow has previously been mentioned in section 1.1, adding the mechanisms of convection to the heat transfer. The convective flow contributes, in general, to a greater heat transfer - but is depended on the injected power rate and flow resistance in fractures (related to hydraulic conductivity). Due to the dependency of injected power rate, the results from a TRT indicating thermosiphon effect must be seen in relation to the final design and operating values of the BTES system. It is also noteworthy that the extent of the effect is larger for a single BHE than for a system of multiple BHE in formation, as several BHE will interact with each other giving a smaller temperature gradient between a specific BHE and the surrounding ground. Gustafsson (2010) recommend multi-injection TRT to detect and determine the influence of natural convective flow. In the study, it was shown that the effect of convective flow influenced both the effective thermal conductivity and the borehole thermal resistance - and that the extent depends on the injection or extraction rate, temperature level, and bedrock type. The

TRT should therefore preferably be performed at rates similar to the operating values of the final system. It was shown that the convective heat transfer was up to 2.5 times higher than that of conductive heat transfer alone. In the case of large regional groundwater flow, one must be aware of the potential large heat losses caused by the water carrying away the heat (Signorelli et al. 2007).

1.3.1 Data analysis using the line-source model

Recorded temperatures and data from the response test can be evaluated with different mathematical models. The analytical infinite line-source model is a fast and simple method, and according to Wilke et al. (2020) the most commonly reported method used for both conventional and advanced TRT. The following section is based on Gehlin (2002) and Signorelli et al. (2007) description on the use of the line-source model to estimate the thermal properties of a BHE.

The analytical model requires simplifying assumptions to adopt the analytical solution of the heat transfer problem between the BHE and the surrounding ground:

- The heat flow around a BHE is represented as an infinite long heat source or sink
- The ground surrounding the BHS is homogenous with uniform thermal properties and initial temperature
- Heat transfer parallel to the BHE axis is negligible, i.e. only heat transfer normal to the BHE
- The thermal process in the surrounding ground is only depended on time and the radial distance from the BHE
- The heat flow process from the collector fluid to the borehole wall, and the resulting temperature loss, is represented by a thermal resistance (R_b)
- Heat transfer mechanism purely by conductive heat transfer. Caution should therefore be made in the case of extensive ground water flow (convective heat transer)

The measured data from the TRT is commonly analyzed with the assumption of a mean fluid temperature:

$$T_f(t) \approx T_{mean}(t) = \frac{T_{up}(t) + T_{down}(t)}{2} \tag{1.4}$$

With T_{up} and T_{down} being the measured fluid temperature entering the TRT rig and after the heating element, receptively.

The line-source method considers the temperature field around an infinite line source as a function of time and radius from the line source (Carslaw & J.C. 1959):

$$T(r,t) = \frac{q}{4\pi\lambda}\int_{\frac{r^2}{4at}}^{\infty}\frac{e^{-u}}{u}du = \frac{q}{4\pi\lambda}E_1(\frac{r^2}{4at}) \tag{1.5}$$

Where

r is the radius from the line source

t is time

q is the heat injection rate per meter borehole length

λ is the ground thermal conductivity

a is the ground thermal diffusivity

and E_1 is the exponential integral function.

E_1 can further be approximated if the thermal front has moved beyond the borehole wall, and the effects of the BHE itself are negligible:

$$E_1(\frac{r^2}{4at}) = -\gamma - ln(\frac{r^2}{4at} - \sum_{n=1}^{\infty}(-1)^n \frac{(r^2/(4at))^n}{nn!} \cong ln(\frac{4at}{r^2}) - \gamma, \qquad for \quad \frac{4at}{r^2} \geq 5 \tag{1.6}$$

where γ is the Euler's constant.

By using Equation 1.5 and 1.6 at the borehole radius ($r = r_b$), and adding the effect of borehole thermal resistance (R_b), the fluid temperature can be expressed as a function of time:

$$T_f(t) = \frac{q}{4\pi\lambda} ln(t) + q(R_b + \frac{1}{4\pi\lambda}(ln(\frac{4a}{r_b^2}) - \gamma)) + T_0 \tag{1.7}$$

Where T_0 in the undisturbed ground temperature, and the fluid temperature T_f corresponds to the mean fluid temperature (Equation 1.4).

For a constant heat injection rate per meter borehole length (q), the last terms of Equation 1.7 is independent of time and becomes a linear relation:

$$T_f(t) = k * ln(t) + m \tag{1.8}$$

Where m is a constant, and k is the slope of the curve and gives the relationship to the ground thermal conductivity (λ):

$$k = \frac{q}{4\pi\lambda} \tag{1.9}$$

Thus, by plotting the change in mean temperature against the natural logarithm of time, the ground thermal conductivity based on the line-source model (λ_{LS}) is given by:

$$\lambda_{LS} = \frac{q}{4\pi} \frac{ln(t_2) - ln(t_1)}{T_{mean}(t_2) - T_{mean}(t_1)} \tag{1.10}$$

Where all temperature measurements between t_1 and t_2 are used to calculate the regression line to estimate λ_{LS}. The first hours of the data from the test must be left out of the calculation of the slope as the beginning of the test only reflects the thermal response of the BHE itself.

The parameters can also be fund using Equation 1.7 with experimental values of the ground thermal conductivity (λ) and borehole thermal resistance (R_b), and compare the best fitting of parameters with the measured temperature development (Gehlin 2002). The measured data may show deviations due to, e.g., solar radiation, but these disturbances may be adjusted for when using the parameter estimation.

2 | Field site description

The studied area is northwest of the city center of Longyearbyen (Figure 2.1). The two boreholes that were drilled during the project are named B1 and B2, where B1 is located on the flat area between Adventpynten and the airport and borehole B2 in the hillside by Blomsterdalen and Veg 700, 40masl.

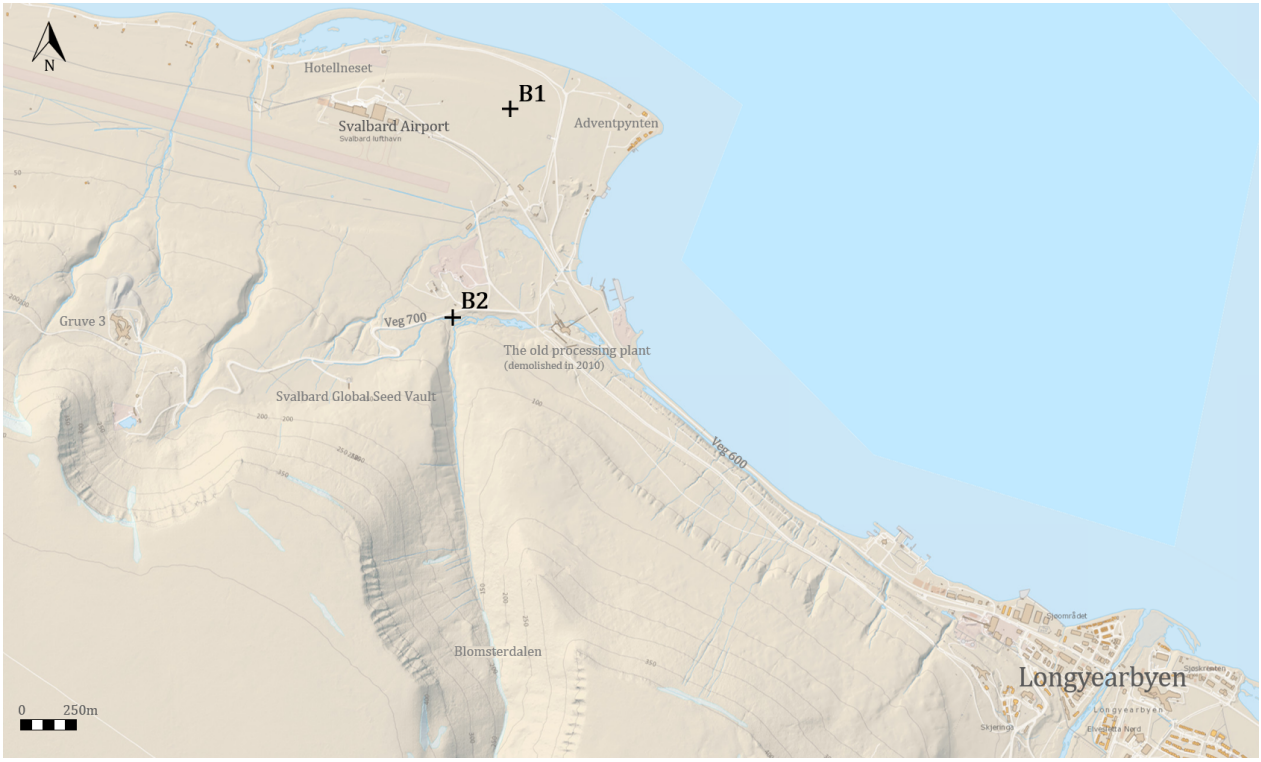

Figure 2.1: Field site location for drilling and Distributed Thermal Response Testing of the two boreholes B1 and B2 i Longyearbyen, Svalbard. Map modified from TopoSvalbard (Norsk Polarinstitutt n.d.*a*).

The ground conditions in Longyearbyen are highly influenced by the presence of permanently frozen ground, i.e., permafrost, and a relatively young sedimentary rockbed covered by sediments and deposits of different origin. On mainland Norway, permafrost is mostly present with a sporadic or discontinuous distribution in high altitude, mountainous areas, and inner parts of Finnmark (Gisnås et al. 2017) - areas sparsely influenced by population and infrastructure. The mainland bedrock is dominated by rocks of Precambrian age together with the nappe complex

of the Scandinavian Caledonides, some smaller areas with Devonian deposits in the west and Permian rocks in the Oslo Graben (Løset 2006). A large extent of the Precambrian rocks are gneiss, as well as granite, other igneous rocks and some arkose. The Caledonian rocks are typically metamorphosed igneous and sedimentary rocks. The Devonian rocks are sandstones and conglomerates, and the Permian are different igneous rocks. This differ the ground conditions and bedrock quality on the mainland considerably from Longyearbyen.

The central Spitsbergen and the geology surrounding Longyearbyen is dominated by sandstone and shale from Middle Jurassic to Early Cretaceous, sandstone and shale from Palaeogene at higher altitudes, and unconsolidated material from Quaternary (Dallmann 2015), see Figure 2.2. According to Piepjohn et al. (2012), the era of Early Cretaous is characterized by changes in sea level resulting in constant shifts between marine and terrestrial conditions. The Early Cretaous deposits are directly overlain by deposits from Palaogene, owing to a hiatus in the sedimentary succession during the Late Cretaous. The bottom of the Palaeogene holds distinct coal seams, which is the basis for the foundation of the mining industry in Longyearbyen. The close to horizontal beds has a regional gentle dip towards southwest, at 1-2 ° near Longyearbyen (Bælum et al. 2012). In connection with the Longyearbyen CO_2 Lab pilot project were it, among several activities, drilled and logged two wells of 518 and 856 m depth next to the road between the city center and Svalbard Airport (Veg 600, close to the old processing plant Figure 2.1). See Figure 2.3 for the stratigraphy in the drill logs, which for the upper 300 m shows; Carolinefjellet Formation (0-150 m), Helvetiafjellet Formation (150-200+), moving into the Janusfjellet Subgroup and Rurikfjellet Formation (Braathen et al. 2012). Olaussen et al. (2019) describes the lithology of the Helvetiafjellet (HF) and Carolinefjellet (CF) formation as: "HF: Massive quartz sandstone, partly conglomeratic passing upward to interbedded sandstone and shale with some thin (cm- to dm-scale) coal beds. CF: Immature sandstone, commonly carbonate cemented (i.e. siderite), and interbedded shale". Pictures of an outcrop in the Carolinefjellet Formation is shown in Figure 2.4. Gilbert et al. (2018) reconstructed the Quaternary sedimentation development in Adventdalen, finding evidence for a thick ice stream advancing during the Late Glacial Maximum - removing previous deposits and forming a subglacial till, muddy glaciomarine sedimentation due to a rapid retreading tidewater glacier in the early Holocene, followed by advancing of a fjord-head delta from early to middle Holocene.

During the drilling campaign for the the CO_2 Lab project, it was identified a water-bearing sandstone aquifer with overpressure in the Lower Cretaous Helvetiafjellet formation (Olaussen et al. 2019). Brackish water with a rate of 125l/min was produced from one of the wellhead.

The same two wells reported by Braathen et al. (2012), were temperature logged (upper 440 m) by the Geological Survey of Norway (NGU) in December 2007. The data is open in the NGU database Permafrost Svalbard (NGU n.d.), according to the fact sheets borehole Dh1 and Dh2 was drilled in September-October and November-December accordingly. Data from the two wells was used to produce the graphs in Figure 2.5, together with minimum, maximum and mean air temperatures recorded at Svalbard Airport in 2007 from Norwegian Centre for Climate Services (n.d.). The Norwegian Centre for Climate Services (NCCS) holds observations and weather statistics from weather stations in Norway, as a national collaboration with the Norwegian Meteorological Institute (MET), the Norwegian Water

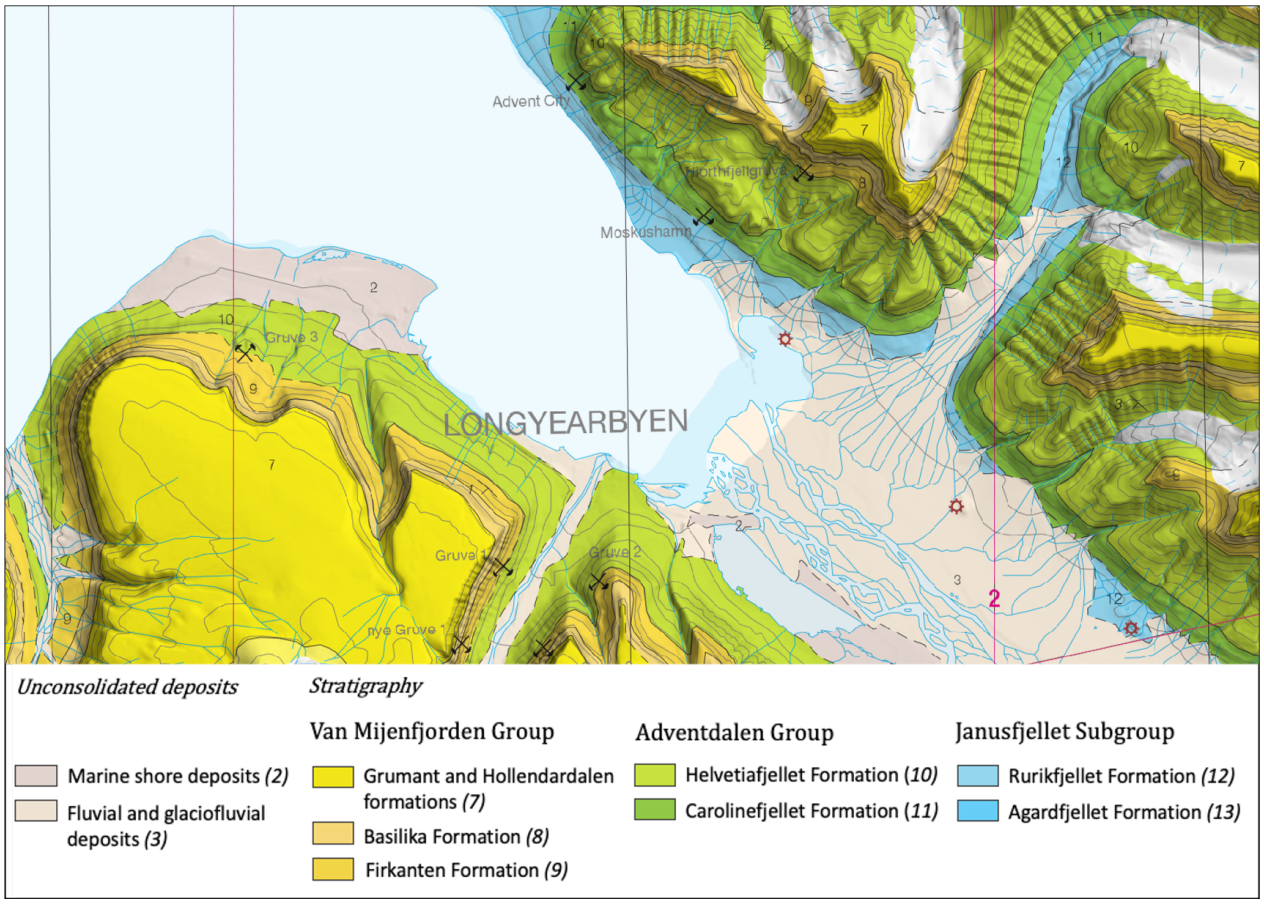

Figure 2.2: Geologic map of Longyearbyen, modified from GeoSvalbard (Norsk Polarinstitutt n.d.*b*) based on Major et al. (2000)

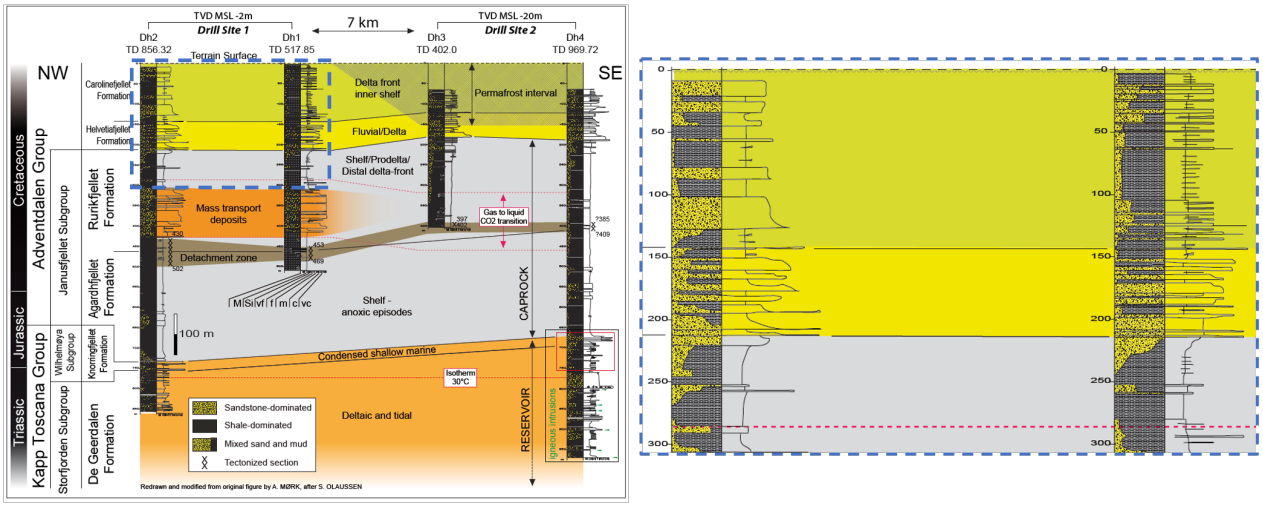

Figure 2.3: Drill logs showing the bedrock stratigraphy from four of the boreholes at the Longyearbyen CO_2 Lab project. The section including the upper 300 m of boreholes "Dh2" and "Dh1", marked with a dotted blue rectangle and enlarged to the right, is assumed representative for the BTES test site. Modified after Braathen et al. (2012).

(a)

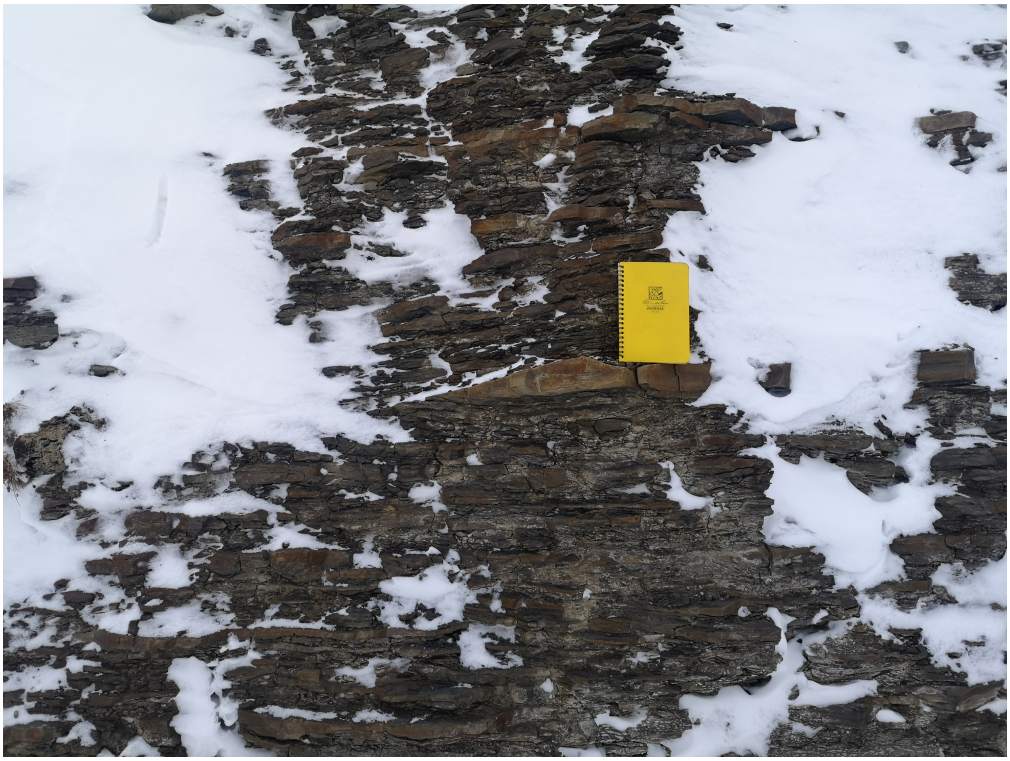

(b)

Figure 2.4: a), b) Outcrop of the Carolinefjellet Formation by the road to the Airport (Veg 600). Photos by Kjersti Buraas Snoen.

Resources and Energy Directorate (NVE), Norwegian Research Centre (NORCE) and Bjerknes Centre for Climate Research. The database includes data from the weather station at Svalbard Airport, Svalbard Lufthavn SN99840, with continuous records from 1976.

From the graphs representing the data from the two wells from the Longyearbyen CO_2 Lab pilot project, named CO_2 free Svalbard by NGU, it was found a gradient of approximate 3.4 $°C/100$m. It is given in the data from NGU (n.d.) that sea water intrudes the boreholes, and the ocean act as a heat source at a distance 100 m from the wells. The wells are separated 15 m apart. Braathen et al. (2012) mention the findings of these temperature measurements as no recognisable permafrost, and that this is consistent with what is reported by Christiansen et al. (2010) for typical thickness of permafrost in Svalbard at the coastline. Furthermore Christiansen et al. (2010) gives typical values of the permafrost thickness to be about 100m in the valleys and 400-500m in the mountains, with the temperature at 15m depth for permafrost in the Adventdalen area to vary from -3.28 to -5.68°C.

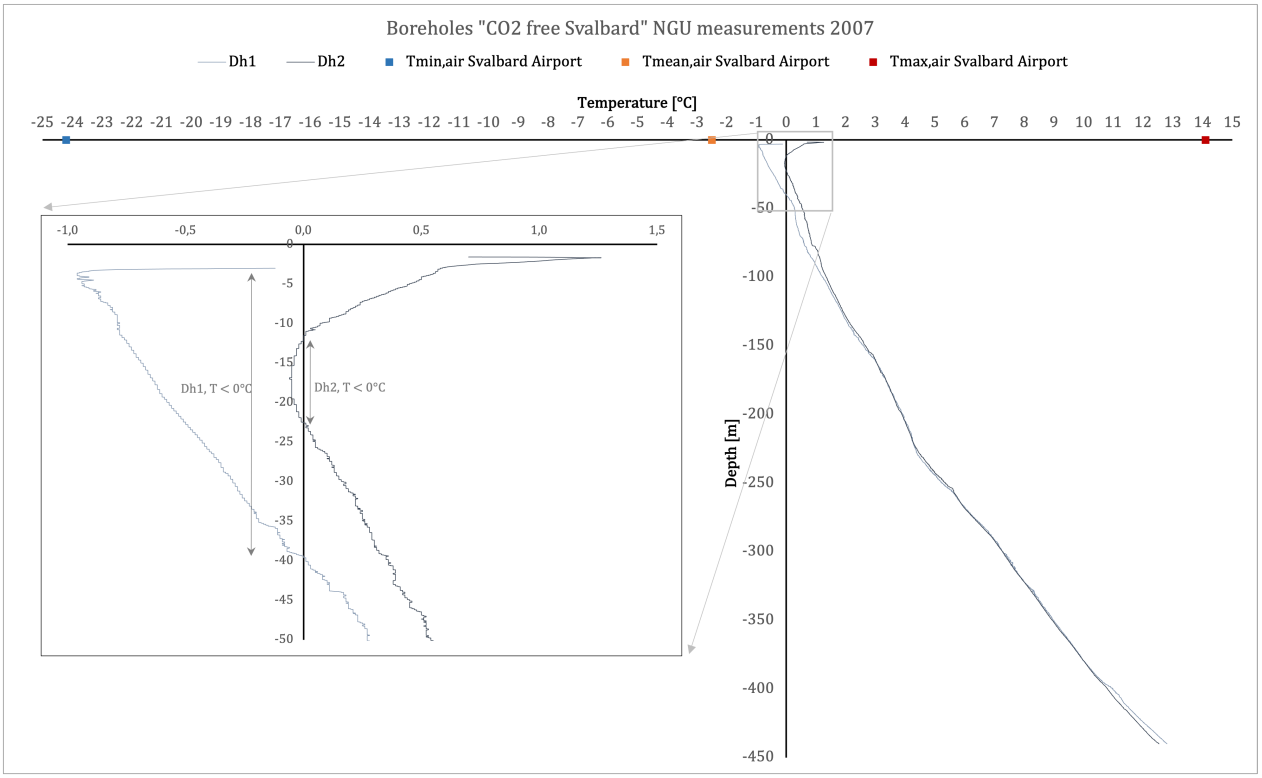

Figure 2.5: Ground temperature and annual air temperatures from 2007 constructed with data recorded by NGU (n.d.) in two boreholes located 100 m from the coast, by the road between the city center and Longyearbyen Airport, and air temperatures at Svalbard Airport (Norwegian Centre for Climate Services n.d.)

According to Christiansen et al. (2010) the thickness of the permafrost in Spitsbergen is typically about 100m in the valleys, and 400-500m in the mountains. Braathen et al. (2012) finds this regional observation consistent with the temperature measurements done in Dh1 and Dh2 by NGU that no recognisable permafrost was found in these coast-near wells.

3 | Methodology - field investigations and data analysis

3.1 Drilling

The drilling was performed by the local contractor Leonhard Nilsen & Sønner (LNS), with guidance from Østlandet Brønn og Energiboring that has long experience with drilling energy wells on the mainland. The two boreholes at 115 mm diameter were drilled by top hammer drilling, flushed with air as medium. The pressured air held a temperature of about 80 °C when leaving the compressor. Steel casing of 140 mm diameter was used in the top layer with soil. The drilling was carried out within the period 8-12.03.2021. See Figure 3.1a-3.1f and Figure 3.2a-3.2e for further details about the involved processes.

Preventive measures for freezing of the borehole water was conducted due to cold air temperatures the time after drilling. In the afternoon Friday 12.03.2021, a tank was filled with 2.5 cubics of water at 55 °C and mixed with 75 kg salt. The water held a temperature of about 30-35 °C when it was filled in borehole B2 (Figure 3.2f). The borehole was filled with approximately 1 cubic of water. It was filled to the top of the borehole casing in several steps, the water table lowered relatively quickly. No measurement of the water table or rate was done.

3.2 Geological material

3.2.1 Sampling drill cuttings

A sample of drill cuttings were sampled for each drill rod during drilling for both boreholes. A bucket was placed next to the drill rig collecting cuttings (Figure 3.1f, 3.2a).

(a) (b)

(c) (d)

(e) (f)

Figure 3.1: a) Remote driving of the drill rig to the site of borehole B2, the valley to the left of the drill rig is named "Blomsterdalen". b) Adjusting of the drill tower for vertical drilling. c) The drill operators from Østlandet Brønn og Energiboring and Leonhard Nilsen & Sønner (LNS) inspecting the drill cuttings to determine if bedrock was reached. d) Welding of the steel casing pipes, two new pipes on the ground in front of the drill rig. e) Inserting of a new drill rod. The air compressor on the left in the picture. The road is named "Veg 700". f) The drill operator from Østlandet Brønn og Energiboring inspecting the drill cuttings. When collecting the samples of drill cuttings, there was placed a bucket in front of the stream and cloud from the mouthpiece of the drill rig. The recess after the bucket is visible to the right in the picture. See also Figure 3.2a.

(a) (b)

(c) (d)

(e) (f)

Figure 3.2: a) A bucket was placed in front of the mouthpiece of the drill rig to collect samples of drill cuttings. b) The U-pipe collector used in borehole B2. The bottom part of the collector (the U-shape) is inside the yellow plastic casing. On the left of the casing is an end weight, the additional weight on top of the coil was also used when installing the fiber. The collector is filled with Kilfrost collector fluid. c) The machine holding the collector during installation, a cap is put on top of the collector. d) Installation of the collector to the right of the drill rig. e) The steel casing marking the top of the borehole, and the collector coming up from the borehole. An additional small pipe was installed together with the collector for temperature measurements with optical fiber cables. f) Lukewarm saline water was filled in the borehole to prevent freezing of the borehole water.

3.2.2 Visual inspection of drill cuttings

The drill cutting samples were visually inspected and described by colour, grain size, and water apparent. From the visual inspection, fifteen samples were picked out for further laboratory examination of the mineral content. The samples were picked out based on the material to represent the majority of the boreholes as well as some of the minor sections with diverging apparent.

3.2.3 XRD

The fifteen samples picked out from the visual inspection were prepared and analysed at the Chemical Mineralogical Laboratory at the Department of Geoscience and Petroleum (NTNU), S.P Andersens veg 13A 7031 Trondheim, within the time 15-23.04.2021.

The samples were firstly placed in glasses and left drying over night in a heating cabinet at 40°C (Figure 3.3a). Once dry, the samples were crushed with a Fly Press Rock Crusher down to a particle size $< 5mm$ (Figure 3.3b-3.3c). To reduce the sample material for further processes, the samples were splitted with a riffle splitter (Figure 3.3d). A Retsch RS 200 Vibratory Disc Mill was used to grind down to a particle size about 10 μm (Figure 3.3e). It was used a 50 ml grinding jar and a disc of wolfram carbide (WC) for the disc mill, and each sample was milled for 1.5 minutes. To round the particles, the McCrone Micronising Mill was used (Figure 3.4a). A topped teaspoon of sample material and 10 ml ethanol were placed in the grinding jar together with 48 cylindrical grinding elements of agate and milled for 2 minutes (Figure 3.3f). The remaining slurry was placed in petri dishes and placed in the heating cabinet at 40°C to evaporate the ethanol (Figure 3.4b). The dried sample materials were firmly filled and smoothed into front-loaded powder holders (Figure 3.4c), and stacked in a magazine keeping all 15 samples (Figure 3.4d). All instruments for the different steps were firmly cleaned with ethanol between each sample to avoid contamination.

A Bruker D8 Advance Serie 2 XRD machine with a cobalt anode tube (λ=1.79 Å) and LYNXEYE detector was used for the analysis (Figure 3.4e). The analysis was run with a X-ray beam angle (θ) from 3-80° with a stepsize of 0.1°.

The resulting diffractograms were qualitatively analysed with the software Diffrac Eva and database PDF 4, and quantitatively analysed with the software Diffrac Topas based on the Rietveld method. A dilute solution of hydrochloric acid (1M HCL)) was used on one sample to confirm the presence of carbonate minerals (Figure 3.4f). The analysis was interpreted by Senior Engineer Laurentius Tijhuis, NTNU.

See subsection 1.2.4 and Equation 1.3 for background of the analysis and explanation of the parameters.

(a) (b) (c) (d) (e) (f)

Figure 3.3: a) The fifteen samples picked out and dried for XRD analysis. From the bottom left, sample ID nr.; 4, 6, 11, 15 19. Middle, left; 24, 27, 33, 38, 42. Upper, left; 45, 53, 54, 62, 66. b) The flypress crusher c) The flypress crusher was used to take the particle size of the samples to <5mm d) Riffle splitter was used to split the samples to reduce the sample material e) A sample after the vibratory disc mill f) A fraction of the sample are placed in a grinding jar with grinding elements of agate and ethanol for the micronising mill.

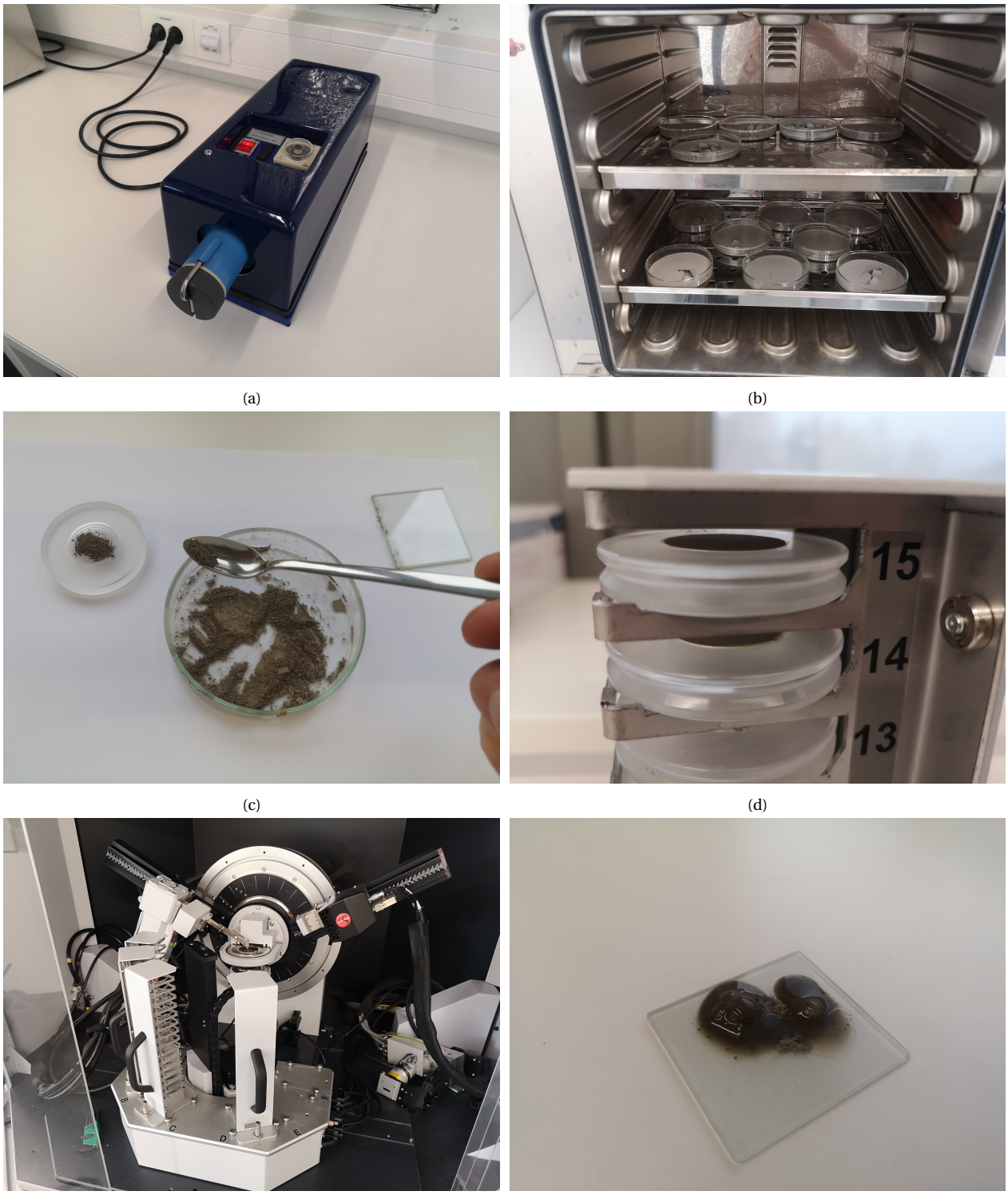

(a) (b)

(c) (d)

(e) (f)

Figure 3.4: a) The grinding jar placed at the front of the micronising mill b) The heating cabinet used for drying the samples prior to preparation, and here to evaporate the ethanol used during the micronising mill process c) Filling the front-loaded powder holders (left), the sample material should be in line with the surface of the holder d) All samples stacked in a sample magazine e) The XRD machine, glass cabinet surrounds the machine. A sample is picked from the magazine and placed in the middle of a spinning plate. X-rays are sent from the left arm at different angles and the detector at the right arm receives the signal after the X-rays have interfered with the sample f) A dilute solution of hydrochloric acid used on a sample containing carbonate minerals.

3.3 Distributed Thermal Response Test

Distributed Thermal Response Test was only performed in borehole B2. If nothing else is specified further in the text, the term "borehole" corresponds to the activity performed in borehole B2.

3.3.1 Set up and procedure

Manual temperature measurements

The ground temperature in the borehole was measured at 5m interval a day prior to test start, at 16.03.2021. A temperature probe attached to a measuring tape was lowered into the collector pipe and the temperature was measured from bottom to top (Figure 3.5c). The same procedure was done 2-3h after test stop.

Installing fiber optic cables

There were installed two fiber optic cables at the inlet (down flow) and outlet (up flow) of the collector U-pipe (Figure 3.5b). It was initially planned to have one fiber optical cable placed in the collector and the other in a small water-filled pipe, but as the small pipe was damaged under installation, it was not possible to fit the cable inside. It was used fiber optic sensing cables of the type *BRUsens Temperature 85°C* from Brugg Kabel AG (2017) connected to the distributed temperature sensor *XT-DTS* from Silixa (2015) with a resolution of sampling per 25cm and 0.01°C.

The optical fiber in the down flow channel recorded for a total of approximate 130h, starting 15h before the heating process of the TRT. Whereas the welded connection to the optical fiber in the up flow channel broke during installation and was firstly set to record after 27.5h after the heating process of the TRT. Data was recorded at a 1min interval, alternating between the two fibers, i.e records at 2min interval for each fiber.

3.3.2 TRT

The TRT test ran from midday 17. until the morning 22.03.2021, in total 114,5h of heating (Figure 3.5a). Prior to heating, a process of purging and circulation of the collector fluid in the system was done. A small leakage in the system caused the pressure in the system to drop slightly during the test period. The test was temporarily stopped, the pressure increased, and started again on six occasions to compensate for the dropping pressure. Temperature and flow data from the test rig was measured at 30 sec intervals.

(a)

(b)

(c)

Figure 3.5: a) The TRT rig from Asplan Viak. Aggregate for power support in the background. The pipe connection between the rig and borehole was firmly isolated with glass wool mats. b) The connection from the collector in the borehole to the TRT rig. The red cables are the optical fiber cables installed inside the collector at the inlet and outlet. c) Manual temperature measurements inside the collector in the borehole after test stop.

3.3.3 Data analysis: Conventional TRT and fiber data

Determining ground water level

The groundwater level was determined based on the information from drilling, and the temperature profiles from manual temperature measurements of the undisturbed ground temperature and 2-3h after test stop. This is based on the assumption that rapid changes in the temperature profile after heating of the borehole are indices of groundwater movement.

Conventional TRT

The data from the TRT was analysed according to Gehlin (2002) and Signorelli et al. (2007) as described in subsection 1.3.1.

The six test stops/starts to adjust pressure in the system cause the temperature and flow to drop. To compensate for this in the analysis, these shorter time periods have been given mean values corresponding to the values before and after.

It was used data from 20h after test start to make the linear regression line to decide the ground thermal conductivity from the linear regression, corresponding to $t_1 = 20h$ and $t_2 = 113.27h$ in Equation 1.10. It was plotted the mean fluid temperature against the natural logarithm of time to get an expression for k in Equation 1.9. The mean added heating effect divided by the effective borehole depth (water filled part of the borehole) was used for the effect per meter (q). The ground thermal conductivity developments have been plotted using the slope value of the mean fluid temperature plotted against the natural logarithm of time, adjusting the slope value as new measurements are added. The developments have been plotted starting from 5h and 20h after test start.

Two different values for undisturbed ground temperature have been calculated; from the circulation process in the Thermal Response Test prior to heating, and from the manual temperature measurements. In the circulation process, the average of the mean fluid temperature during the circulation has been used. For the manual temperature measurements, it was used the mean value of the temperature measured prior to test start, with the mean calculated from what was assumed as the water filled part of the borehole. The value of undisturbed ground temperature has further been used for the estimation of borehole thermal resistance.

The borehole thermal resistance has been estimated plotting the mean value of the collector fluid as fluid temperature and using Equation 1.7 for two different values of the undisturbed ground temperature (T_0). A ground volumetric heat capacity (c_V) of 2020kJ/(m^3,K) has been used together with λ_{LS} for the ground thermal diffusivity (a) (Equation 1.1). The diameter of the borehole was set to 115mm (Table 4.1). Different values of R_b has been used in Equation 1.7 and plotted, to estimate the curve with the best fit to the fluid temperature measured from the test.

The heat injection effect (Q) was calculated from the specific heat capacity (C_p) and density(ρ) of the collector fluid

(Kilfrost), the measured volumetric flow ($\dot{V}$) from the TRT rig and the absolute value of the temperature difference (ΔT) from the fluid leaving (flow down) and entering (flow up) the TRT rig (see Equation 3.1). The effect per meter effective borehole depth (q) was set as the mean effect calculated from the flow (Q_{mean}) divided by the the effective collector length - set as the collector length (198 m) subtracting the bottom weight (1 m) and the groundwater level.

$$Q = C_p \rho \dot{V} |\Delta T| \tag{3.1}$$

Temperature analysis of the optic fiber records, DTRT

The DTS logger connected to the two fiber optic cables placed inside the borehole collector tube at the down flow and up flow produces a raw file for each measurement for a set length of the fiber including more than the depth of the borehole.The length of the fiber is in the analysis and further in the thesis described as the depth of the borehole. All raw files were stacked together and measurements exceeding the borehole was removed using a Matlab script.

To represent a temperature at a specific depth, it was used mean values for a 10m section, e.g. the value at 10m depth corresponds to the mean value from records from 5 to 15 m depth of the borehole. The same depth sections were used for further analysis, calculating the effect and thermal conductivity at depth, as well as ΔT during recovery. It has only been used relative temperature differences as the records from the fibers have not been calibrated to an environment with known temperature. Records from the two fibers have been adjusted to each other based on the best fit of values of the records from the bottom of the borehole.

The effect (Q) at depth was calculated by using Equation 3.1 with the specific heat capacity and density of the collector fluid (Kilfrost), the mean value of the volumetric flow from the TRT rig and the absolute value of the temperature difference between the two sections, e.g. ΔT=T(10m depth)-T(20m depth), during the heating process of the TRT. The effect (Q) was calculated from both the down flow and up flow. A total value for the effect at each section was made by adding the contribution from both the down- and up flow. The effect per meter (q) was calculated by taking the effect (Q) divided by the distance between the depth sections used for ΔT (10m).

Thermal conductivity at depth was calculated in the same way as the conventional TRT analysis (see Equation 1.9) by taking the slope (k) of the linear regression line when plotting ln(t) (neglecting the first 20h of the test) against temperature for both the down- and up flow, using it together with q at the specific depth as described in the previous paragraph.

3.4 Numerical modelling in GeoStudio 2021 R2 - TempW

Four 2D models simulating the processes prior to, during and after Thermal Response Test at 100m depth were done using the Seequent software GeoStudio 2021 R2 Temp/W. Reports of the four models with input parameters and specifications are given in the Appendix. Figure 3.6 displays the set-up of the four models.

The four models involve one steady-state analysis and three transient analysis, the models are accordingly named; Steady-State initial air, Transient initial water, Transient TRT test, Transient TRT recovery. The transient analysis initial temperatures are given from the last step results of the previous analyses. The models have an element thickness of 1m, modelled with two regions given different material properties; a 6x6m square (Region 1) and a circle with 115mm diameter (Region 2). Three different materials were defined, named; bedrock, air and borehole water. Three different thermal boundary conditions were defined as; T_0, Water and Heat injection.

The assigned material properties of the defined material are given in the reports in the Appendix. The "Bedrock" material was given the ground thermal conductivity found from the temperature analysis of the optical fiber recorded at 100m depth.

The boundary conditions "T_0" and "Water" was constant and set to -1.7°C and 3.0°C, respectively. The value for "T_0" was set to correspond to the manual measurements of the undisturbed ground temperature at 100m depth. The value of 3.0°C for the "Water" boundary condition was chosen as a value above the freezing point of water. The "Heat injection" boundary condition was set to a function type, with the input function as the time and temperature records from the optical fiber at the 100m depth section during the TRT test and adjusted with +2°C.

The Steady-State initial air had a time duration of 30 days. The intention of the model was to simulate the undisturbed ground temperature of the surrounding ground, giving all nodes the initial temperature "T_0" and further serve as basis for the next analyse. Region 1 was assigned the material properties of "Bedrock" and Region 2 "Air". The boundary condition "T_0" was set at the circumference of Region 1. Region 1 was assigned the "Bedrock" material and the boundary condition "T_0" at the circumference of Region 1 throughout the three next models.

The Transient initial water had a time duration of 7 days, with a linear step increase of 15 steps (0.5d time increment). The material of Region 2 was set to "Borehole water", with the boundary condition of "water" at the circumference of Region 2. The intention of the model is to simulate the natural filling of groundwater in the borehole after drilling. Region 2 was kept assigned the material "water" for the two next models.

The intention of the Transient TRT test was to simulate the response of the TRT test, and the recovery with the Transient TRT recovery model. For the Transient TRT test was the boundary condition set to "Heat injection" at the circumference of Region 2. In the Transient TRT recovery model had no boundary condition at the circumference of Region 2. The time duration of the Transient TRT test was set to 114.5h, with a linear increase of 458 steps (15min time increment). The duration of the Transient TRT recovery was set to 30 days, with an exponentially step increase of 150 steps with an initial increment size of 15min.

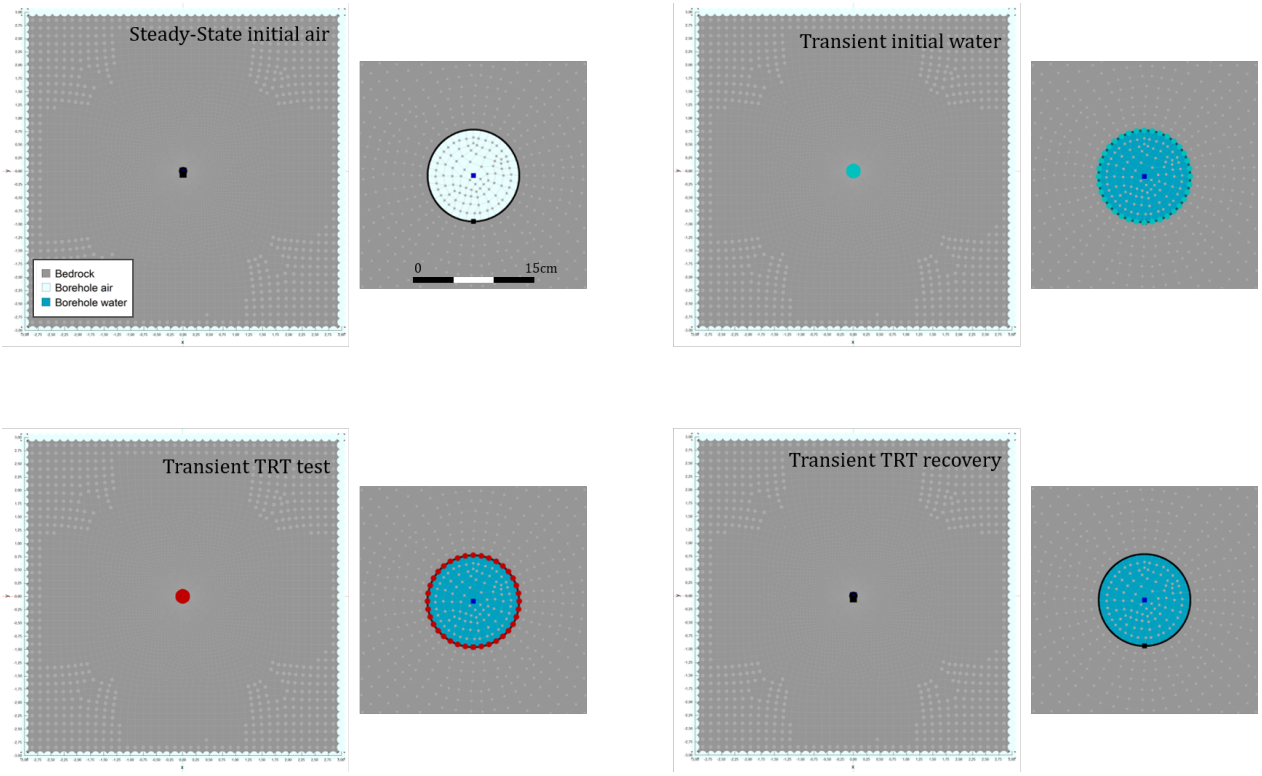

Figure 3.6: Set up of four numerical models in GeoStudio 2021 R2 TempW with geometry, materials, boundary conditions and mesh distribution. Each model is displayed with the modelled area of 6x6m (Region 1) and a zoomed section of the borehole (Region 2) to the right. All models were run with a constant boundary condition of -1.7°C at the circumference of Region 1. The transient initial water model was run with a constant boundary condition of 3°C at the circumference of Region 2. The Transient TRT test model was run with a function type boundary condition, corresponding to the temperature development from the optical fiber records at 100m depth, at the circumference of Region 2.

4 Results

4.1 Drilling

Details of the drilling and boreholes are listed in Table 4.1. Additional information with drill log from Østlandet Brønn og Energiboringare and field notes are found in the Appendix.

Borehole B2 was drilled 08-09.03.2021. Bedrock was reached at about 6 m depth. It was used steel casing from 0-12 m depth. There were wet drill cuttings and water between 6-9 m depth. The drilling on Monday 8^{th} was paused overnight at 12 m depth. During the night the water level had risen several meters, the water was not frozen (Figure 4.1a). The dust cloud from drilling showed that the stratigraphy of the bedrock had changing layers; light dust at layers with greater drilling resistant, brown and grey dust at layers with less drilling resistance. It was typically encountered several layers during one drill rod (3 m) (Figure 4.1b). It was in average drilled for 3min and 37sec per drill rod. At 150 m, there was a smaller water intrusion, with the following drill cuttings being wet. The water amount increased at about 165 m depth, with a presumed water intrusion of 500-600 l/h (visually determined by the drill operator from Østlandet Brønn og Energiboring). Additional increase in water at 174 m depth presumed 500-1000 l/h. At 186-189 m, there was a pocket at the end of the rod, followed by a transition of the bedrock. There was black marbling in the water from the borehole (Figure 4.1c). The borehole was drilled to 198 m depth. The borehole was flushed and rinsed, according to the drill operator, the water tasted saline.

Two hours after the drilling was stopped, the water table was presumed to be at 60 m depth. Half an hour later, the level had risen to be at about 40 m depth. This was presumed by dropping a gravel and counting the seconds before it hit water.

A single U-collector pipe and a small empty pipe for installing fiber optic cable were installed in the borehole in the evening (09.03.21). The smaller additional pipe was damaged under installation when the weight of the collector pipe was too much for the machine to hold back and the lowering of the pipes went out of control for a short time.

According to the drill operators, it is normal that air is released from the borehole after drilling as it is used pressured air during drilling (Figure 4.1d). A rumbling sound was heard from the borehole the following day, geologists from UNIS and Store Norske Spitsbergen Kulkompani AS proved methane gas was leaking from the borehole on 10.03.21.

Table 4.1: Specifications for the boreholes drilled in Longyearbyen for Distributed Thermal Response Tests.

Description	**B2, Blomsterdalen**	**B1, Hotellneset**
Drilling date	08-09.03.2021	11-12.03.2021
Drilling depth [m]	198	57
Drilling direction	Vertical	Vertical
Borehole diameter [mm]	115	115
Depth to bedrock [m]	6	>57
Casing length [m]	12	48
Casing diameter [mm]	140	140
Length collectortube*[m]	197	
Collector type	Single U-pipe, 40 mm	
Collector fluid	Kilfrost: $\rho = 1195 kg/m^3$, $c_p = 3046 J/(kg,K)$	
Groundwater level [m below surface]**	40	
Effective length of collector [m]	157	

* Excluded bottom weights (1m)
** Determined from data analysis

The gas bubbling had stopped by midday 11.03.21.

Borehole B1 was drilled 11-12.03.2021. The drilling was stopped at 57m depth, when the bedrock was still not reached. Steel casing was used from 0-48m. Representative material encountered in the borehole are shown in Figure 4.2. There were no water intrusion during drilling, but some ice particles was observed at 12-15m depth and slightly moist cuttings at 27-30m depth. The drill cuttings were moist from 48m depth.

4.2 Geological material

4.2.1 Visual inspection of drill cuttings samples

The 66 samples collected during drilling was visually inspected indoors some days after drilling, photos of the samples are given in Figure 4.3 with the corresponding sample ID nr., where nr. 1 is at the top of borehole and nr. 66 at the bottom of the borehole. Each sample represents one drill rod of 3m.

The majority of the samples were dry, expect for at the top and bottom of the borehole. Sample nr. 1-3 had a moist apparent, nr. 4 and 5 were wet, nr. 6 had some moisture. Sample nr. 7 to 53 were dry, and sample nr. 54 to 66 were wet. Some changes in colour can be seen from Figure 4.3, the top six samples had a brown to brown-grey colour, the majority has a grey colour with some lighter and darker samples in between, at the bottom of the borehole (from sample nr. 51) the samples were dark grey.

4.2.2 XRD

The resulting mineral content and distribution from the XRD analysis are listed in Table 4.2, and visually presented in Figure 4.4. These are based on the interpreted diffractograms given in the Appendix, listed and labelled with

(a) (b)

(c) (d)

Figure 4.1: a) Flushing of the water encountered at the top of borehole B2. b) Different colour apparent of the dust cloud from drilling, to the far left the cloud is darker with a more brown-grey colour compared to the dust closer to the drill rig with a light grey coloured look. c) Dark marbling in the water from the borehole from one of the last drill rods. d) Air and gas leaking from the borehole after drilling. It was later proved methane was leaking from the borehole.

(a) (b)

Figure 4.2: a) Sediments deposits representative for the upper 15m of borehole B1 b) Sediment deposits typical for 15-57m depth of borehole B1, additionally with some layers of sand.

Figure 4.3: Drill cuttings samples collected during drilling with ID nr., with nr. 1 being at the top of the borehole (0-3m depth) and nr. 66 at the bottom of the borehole (195-198m depth). The sampling bags are 5l bags, placed on a table.

ID as in Table 4.2. In Table 4.2 the mineral content is given as percentage of the crystalline material, whereas Figure 4.4 presents the mineral content as percentage of the total sample - taking the crystalline/amorphous-part into consideration.

The percentage of crystalline material in the samples varies from 45-71%. With the largest percentage of crystalline material at 96-99m depth and at the bottom of the borehole (195-198m). The smallest percentage of crystalline material is at 156-159m depth. Most of the samples has a percentage of crystalline material in the range of 50-59%.

The mineral content is further described as the mineral content as percentage of the total sample, as presented by Figure 4.4.

Quartz is the most dominating mineral in all samples, ranging from 17-37% with a mean content of 23%. The five samples with the largest quartz content (24-37%) is found at 96m depth and below; having two distinct peaks at 96-99m and 132-135m depth, and an increasing amount towards bottom of the borehole. The smallest quartz content (17%) is at the top of the borehole (9-12m) and at 111-114m depth. The rest of the samples varies slightly with a quartz content around 20%.

The fieldspar content varies from 8-26% with a mean content of 13%. The most significant contribution is found at 96-99m depth with a fieldspar content of 26%, whereas the next largest content is 16% at 54-57m depth. The upper part of the borehole has in general a larger content, than the other half.

The mean content of mica is 11%, varying in the range 7-15% throughout the whole borehole depth. The greatest contributions of 15% is at 69-72m and 9-12m depth.

Clay minerals and siderite both have a mean content of 3%. Clay minerals are present in all samples, siderite is present in twelve of the fifteen samples. Clay minerals have the largest content (5%) at the bottom of the borehole (195-198m) and 132-135m depth, and the smallest content at 111-114m and 156-159m depth. The contribution of siderite is greatest in the samples from 111 to 159m (5-7%).

Pyrite is present in nine of the samples, evenly distributed at the depth of the borehole around the mean content of 1% except for a peak content of 4% at 159-162m depth and 3% at the top of the borehole (9-12m). Calcite is only present in four of the samples, giving a mean content of 1% - but the contributions are of 5% at 111-114m and 15-18m depth, 3% 54-57m depth and 1% at 156-159.

4.3 DTRT

4.3.1 Temperature profiles

Temperature profiles from manual temperature measurements, records from the optical fiber and mean temperature of sections from the optical fiber measurements are presented in Figure 4.5. The manual temperature measurements are done prior to test start (approximate 24h), as a representation of the undisturbed ground tempera-

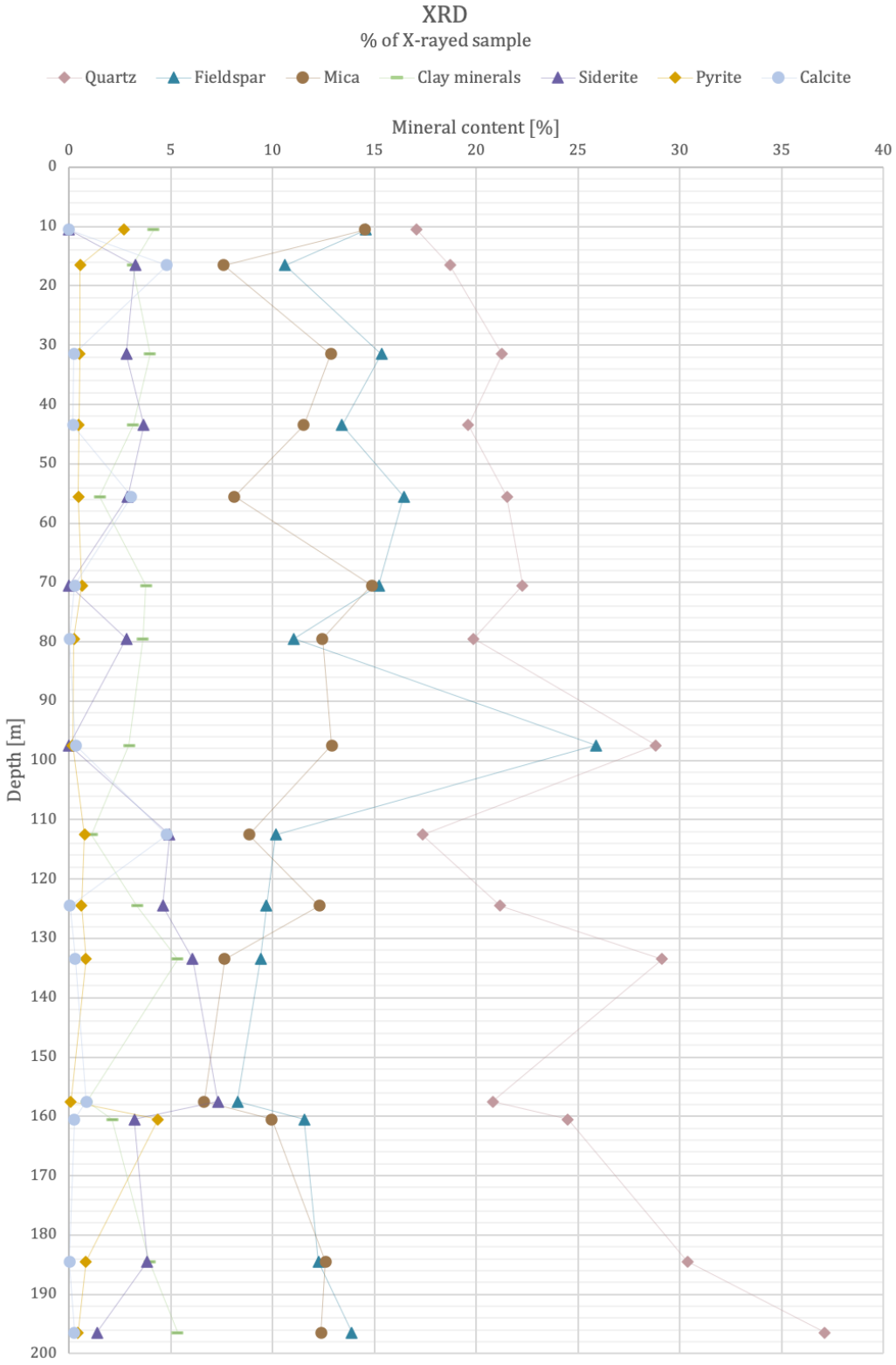

Figure 4.4: Mineral content and distribution of fifteen drill cuttings samples from borehole B2 at different depths, analysed with X-Ray Diffraction (XRD) method. The interpreted contents from the XRD-analysis are weighted against the crystalline component of each sample.

Table 4.2: Mineral content from X-ray diffraction analysis of drill cuttings samples from borehole B2.

ID	Depth		Mineral content [% of crystalline material]												[% of x-rayed sample]	
	Top	Bottom		Fieldspar		Mica		Clay minerals							Crystalline	Amorphous
			Quartz	Albite	Microcline maximum	Muscovite 2M1	Biotite 1M Mica	Chlorite IIb	Kaolinite (BISH)	Pyrite	Calcite	Siderite	Halite			
4	9	12	32.19	21.85	5.66	27.41		4.43	3.38	5.07					53	47
6	15	18	38.19	20.20	1.45	15.50		4.10	2.27	1.09	9.78	6.64			49	51
11	30	33	37.30	23.95	2.96	22.54		4.35	2.63	0.93	0.41	4.93			57	43
15	42	45	37.69	24.40	1.37	22.15		4.47	1.58	0.92	0.37	7.06			52	48
19	54	57	39.80	26.06	4.36	15.04		2.58	0.20	0.85	5.66	5.33	0.12		54	46
24	69	72	39.05	24.36	2.32	26.08		5.18	1.44	1.09	0.49				57	43
27	78	81	39.73	19.74	2.34	24.87		5.91	1.31	0.47	0.02	5.61			50	50
33	96	99	40.57	30.37	6.05	18.17		2.32	1.84	0.23	0.46				71	29
38	111	114	36.16	18.59	2.54	18.41		2.18	0.11	1.58	10.02	10.25	0.15		48	52
42	123	126	40.74	15.62	3.02	23.64		2.79	3.62	1.16	0.08	8.86	0.49		52	48
45	132	135	49.35	8.78	7.15	12.93	0.01	0.37	8.64	1.39	0.51	10.27	0.60		59	41
53	156	159	46.23	17.43	0.94	14.39	0.34	1.83	0.10	0.17	1.89	16.25	0.44		45	55
54	159	162	43.73	19.05	1.58	17.77		2.04	1.75	7.80	0.46	5.71	0.10		56	44
62	183	186	47.46	12.15	6.97	19.67		1.45	4.71	1.28	0.03	6.01	0.26		64	36
66	195	198	52.27	12.84	6.71	17.44		2.39	5.10	0.61	0.37	1.92	0.34		71	29

ture (T_0) and 2-3h after test stop. The profiles from the optical fiber is 15h prior to test start, and 2h after test stop measured in the down flow collector. In addition there is plotted a line for the assumed water level at 40m depth, and the mean value of the manual measurements of the undisturbed ground temperature from 40m depth.

The manual measurements of the undisturbed ground temperature (T_0) have a starting value of -4°C at the top of the borehole, the temperature is rising to -1° at 13m depth before it decreases again. From 40-750m depth the temperature is close to constant around a value of -2.2°C. From 80m depth the temperature is increasing with a linear trend to a temperature of 1.2°C at the bottom of the borehole, a gradient of 2.8°C/100m. The mean value of T_0 from the manual measurements from 40m depth and to the bottom of the borehole is -0.97°C. The temperature is passing 0°C, from negative to positive temperatures, at 160m depth. The mean value of all measurements is -1.14°C, and the mean value of the measurements from 40m depth is -0.97°C.

The manual measurements 2-3h after TRT have a starting value of 1.4°C at the top of the borehole, with rising temperature to a value of 2.3°C at 14m depth before it decreases to 1.6°C at 34m depth. Followed by a rapid increase to 4.4°C at 50m depth. From 50m depth the temperature is fluctuating in the range 4-5°C until it increases and reaches the highest value of 5.6°C at 179m depth, and thereafter decreases to the bottom of the borehole ending at 4.0°C.

The two profiles from the optical fiber follows the same trend as the manual measurements, with a difference between the profiles om approximate 1-1.5°C for the profiles of undisturbed ground temperature and 2.5-3.5° of the profiles after test stop.

4.3.2 Conventional TRT

The temperature development of the collector fluid together with the air temperature inside and outside the TRT rig recorded during the circulation and heating process of the Thermal Response Test (TRT) are presented in Figure 4.6, and a more detailed section of the circulation process in Figure 4.7. The down flow, up flow and mean temperature of the collector fluid are presented.

During the circulation process, the temperature difference between the down flow and up flow of the collector fluid is less than 0.5°C with the down flow being colder than the up flow. The average of the mean temperature

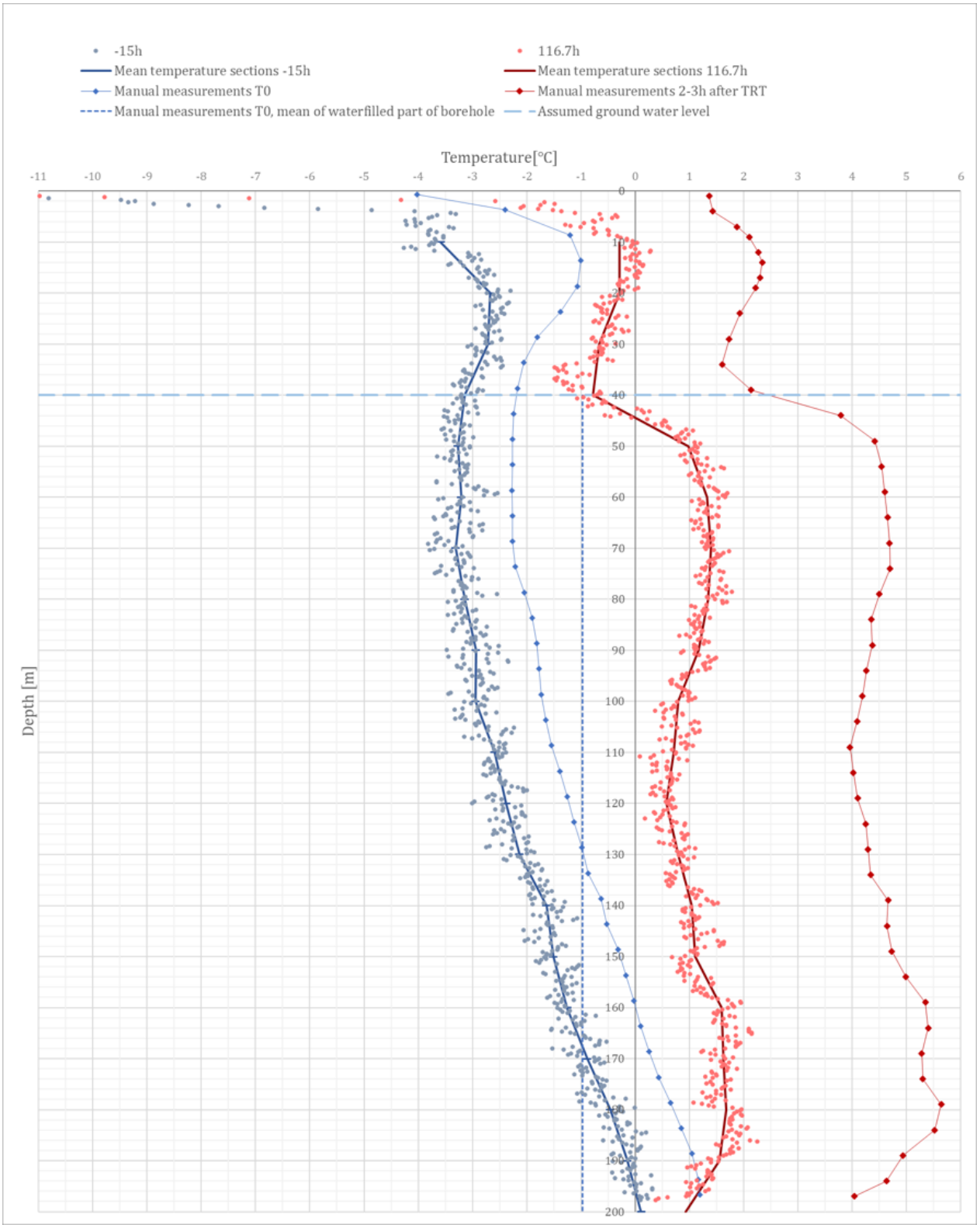

Figure 4.5: Temperature profiles prior to and after TRT from optical fiber records (dots), mean values of 10m sections of the optical fiber records (solid lines), and manual measurements (solid line with indicator).

is -3° during the circulation process, excluding the first few measurements at the beginning of the process. The temperature of the collector fluid down flow instantly increases about 4°C at test start, while the collector fluid up flow is almost constant at the beginning of the heating process.

The temperature development of the collector fluid is more rapid in the beginning, with the slope reducing after 20h, after 35h the slope is almost constant. At the end of the test the collector fluid has a mean temperature of 9.2°C. On six occasions there are short deviations from the temperature development of the collector fluid, seen as outliers in the graphs.

The outdoor air temperature measured under the TRT rig is at about -20°C at test start and the first 15h of the test, thereafter there is an significant increase in temperature to around -2°. 55h after test start the outdoor air temperature is decreasing again and stabilizing around -10° from 80h and to the end of the test. The graph representing the air temperature inside the TRT rig follows the same trend as the outdoor air temperature, but has some slightly more fluctuations.

The circulation flow ($\dot{V}$) and added heating effect (Q) during the TRT test is displayed in Figure 4.8. The measurements from both of the parameters are relatively constant around a mean flow of 0.5l/s and mean added heating effect of 7.8kW, except six deviations with the same behaviour and time as mentioned for the temperature of the collector fluid.

The linear regression line fitted to the plot of the mean fluid temperature against the natural logarithm of time, from 20h after test start, gives a slope of 1.1715 (Figure 4.9). Given a ground water level at 40m depth resulting in an effective length of the collector as 157m (Table 4.1), and a mean added heating effect (Q) of 7.8kW this gives the effect per meter effective borehole depth (q) to be 49.7W/m. The slope value of 1.1715 and q=49.7W/m inserted in Equation 1.9 and 1.10, gives a value of the ground thermal conductivity from linear regression (λ_{LS}) to be 3.4W/(m,K). The value of the ground thermal conductivity from linear regression is plotted together with the ground thermal conductivity development throughout the test in Figure 4.10. The ground thermal conductivity development increases during the test, at the end of the test the development starting at 5h after test start reaches a value of about 3W/(m,K). The ground thermal conductivity development starting at 20h after test ends at the value from linear regression (λ_{LS}) at 3.4W/(m,K).

The estimates for borehole thermal resistance based on two different values of the undisturbed ground temperature (T_0) are given in Figure 4.12 and 4.11. For an undisturbed ground temperature of -3.0°, the measured mean fluid temperature fits with the curve corresponding to R_b=0.1(m,K)/W (Figure 4.12), and an undisturbed ground temperature of -0.97° fits with the curve corresponding to R_b=0.06(m,K)/W (Figure 4.11).

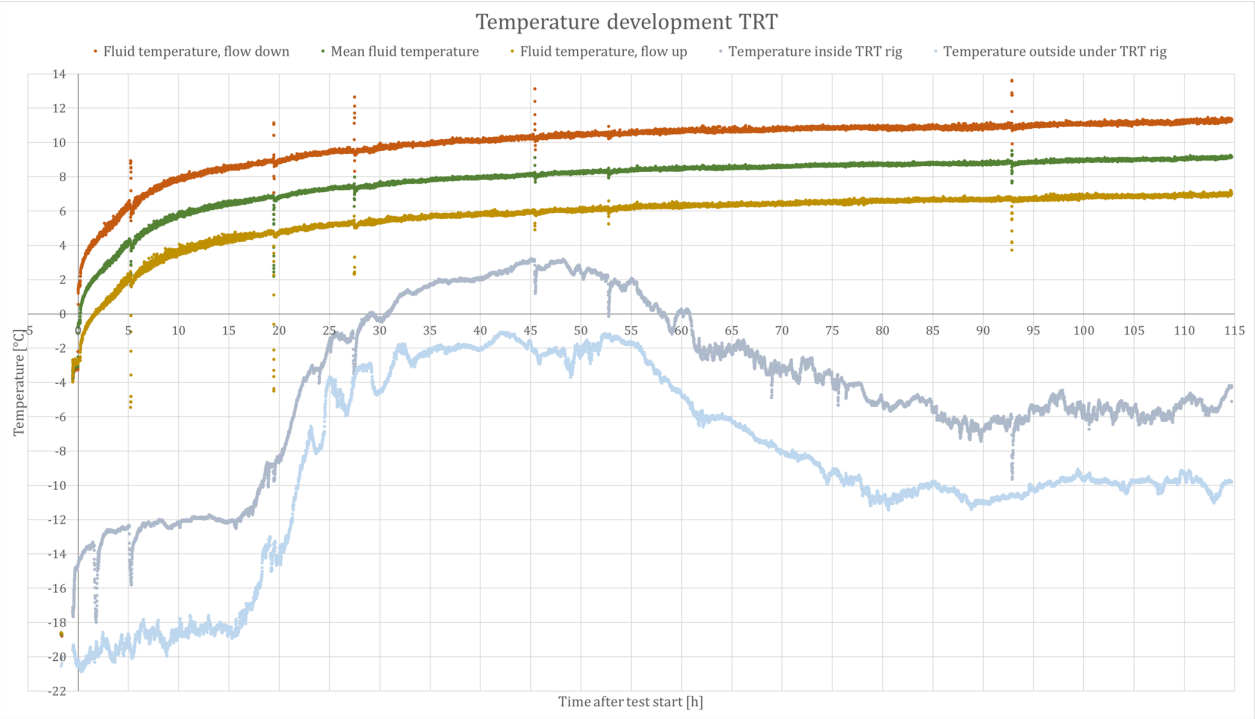

Figure 4.6: Surrounding temperature and temperature development of the collector fluid during Thermal Response Test (TRT) in borehole B2. The figure is based on a template from Asplan Viak.

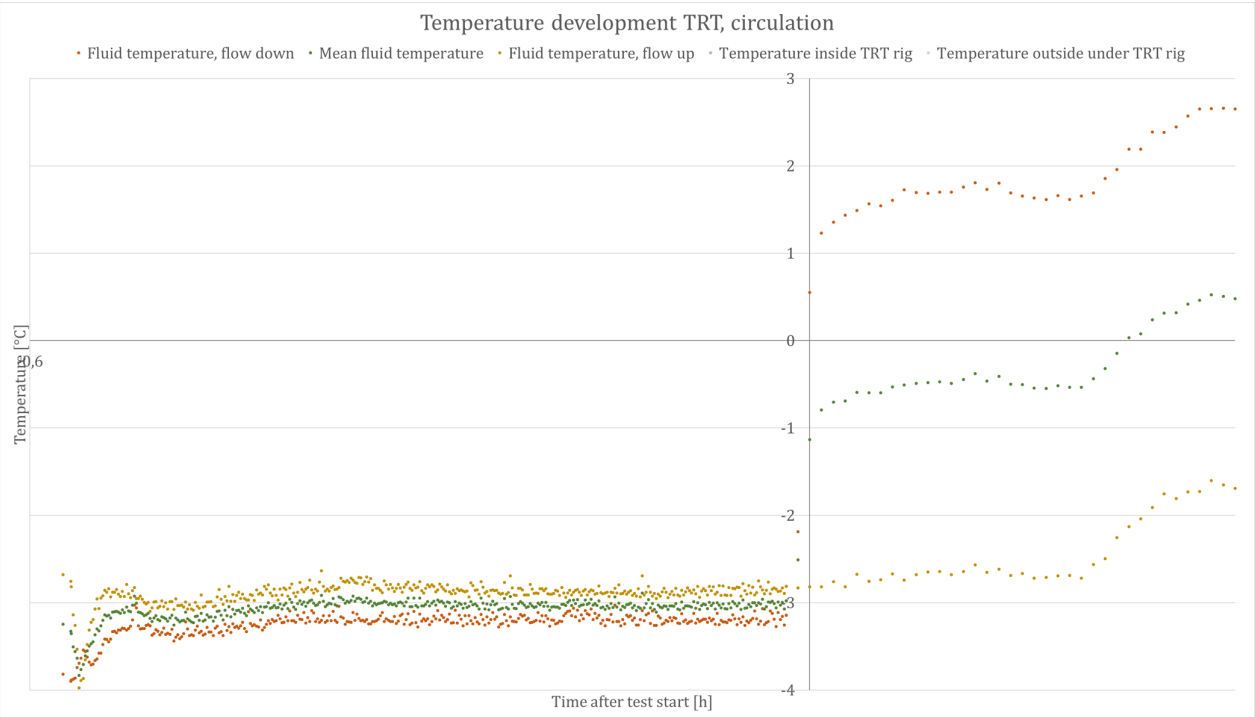

Figure 4.7: Temperature development of the collector fluid during circulation and immediately after heat start. The figure is based on a template from Aslan Viak.

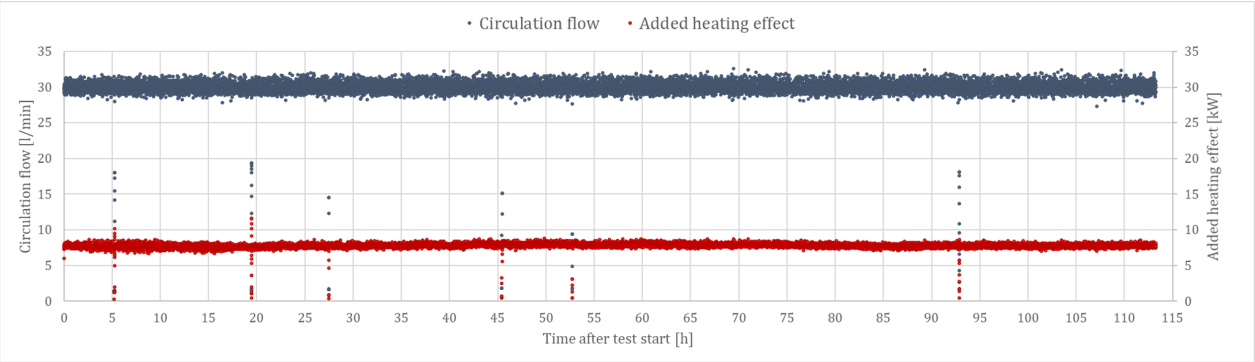

Figure 4.8: Circulation flow and added heating effect during TRT. The figure is based on a template from Asplan Viak.

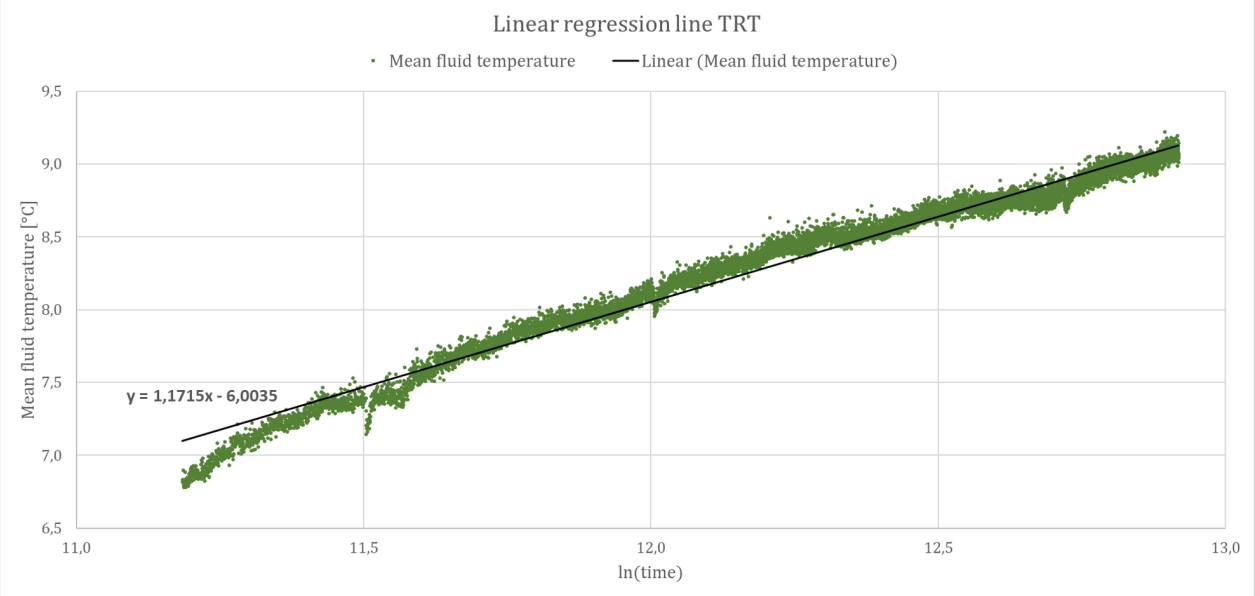

Figure 4.9: Linear regression line fitted to the mean fluid temperature of the collector fluid plotted against the natural logarithm of time during TRT, excluded the first 20h of the test. The figure is based on a template from Asplan Viak.

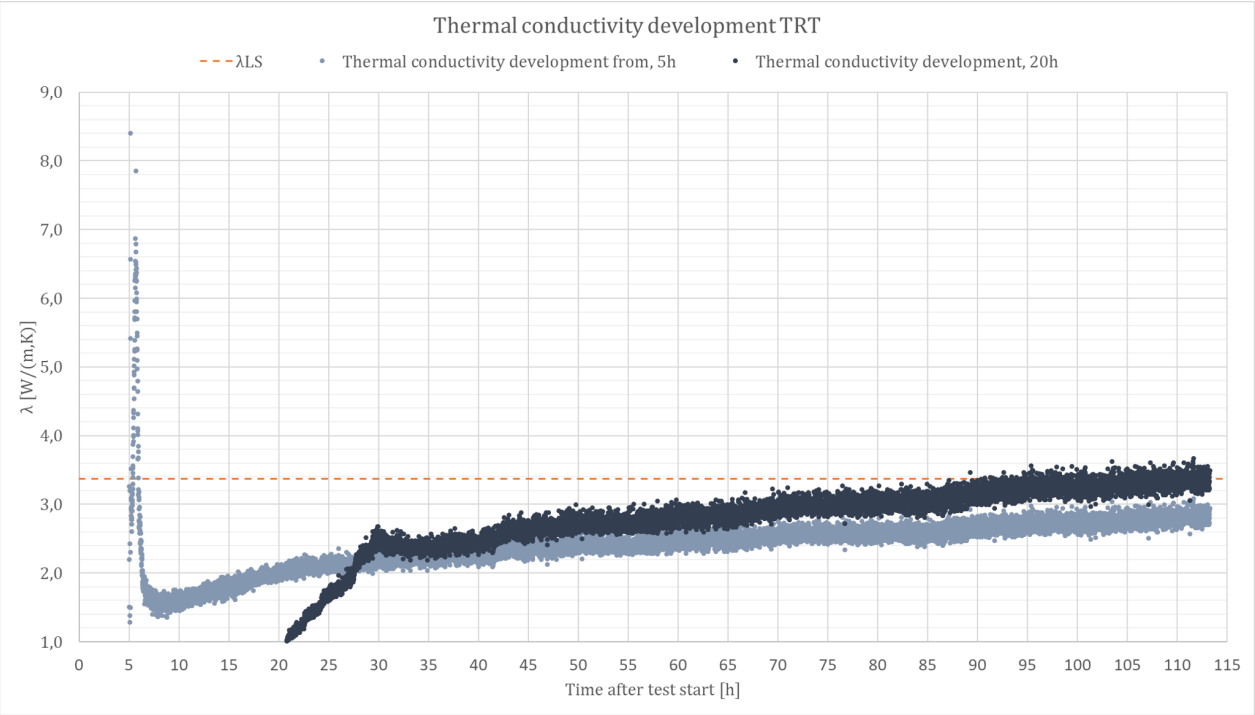

Figure 4.10: The thermal conductivity development during TRT, and the value of the calculated thermal conductivity from linear regression. The figure is based on a template from Asplan Viak.

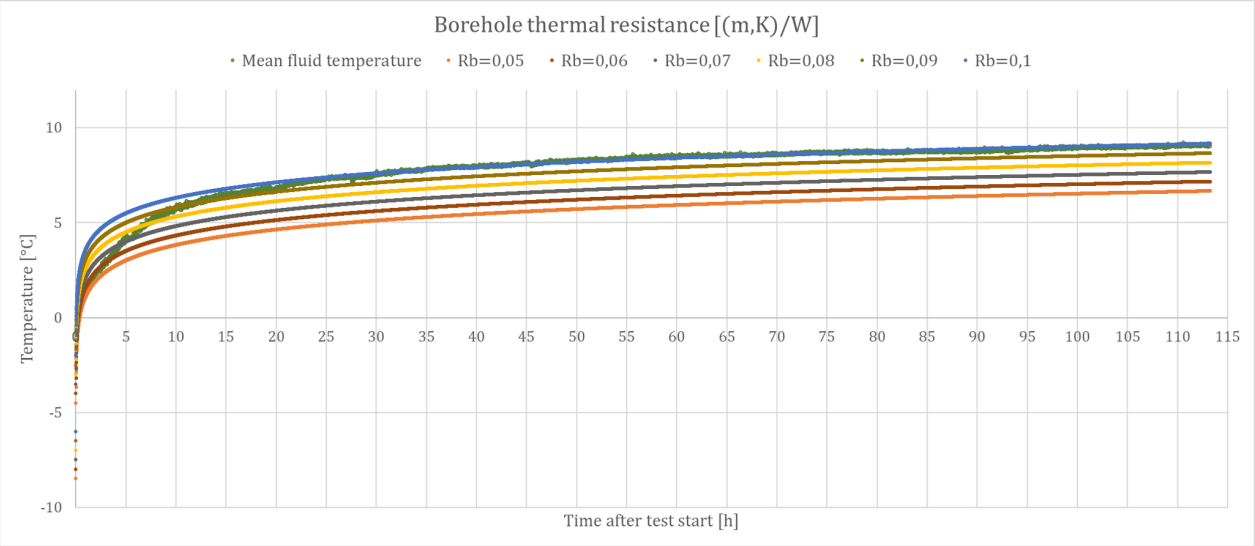

Figure 4.11: Best fit parameter adjustment of the borehole thermal resistance (R_b) during TRT given an undisturbed ground temperature (T_0) of -3.0°C. The figure is based on a template from Asplan Viak.

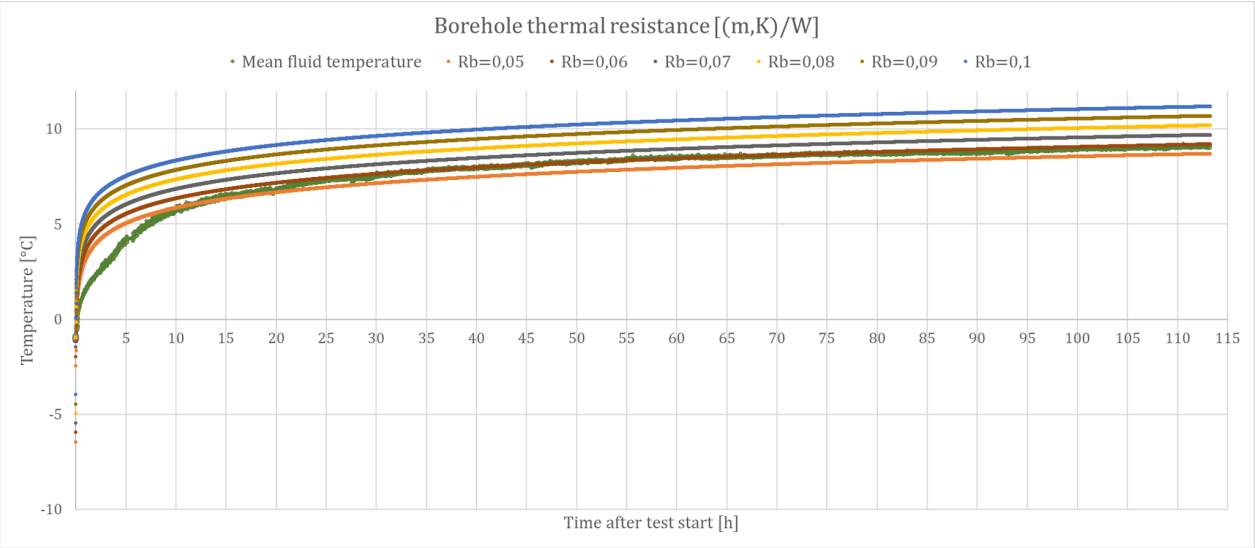

Figure 4.12: Best fit parameter adjustment of the borehole thermal resistance (R_b) during TRT given an undisturbed ground temperature (T_0) of -0.97°C. The figure is based on a template from Asplan Viak.

4.3.3 Fiber data

The temperature developments at depth from the optical fiber measurements in the down flow and up flow collector channels are presented in Figure 4.13, with a detailed section of the -5h prior to test start in Figure 4.14 and the recovery after test stop in Figure 4.15. Data from the up flow channel from 27.5h after test start have a linear increase in temperature at all depths. The temperature difference from the bottom (190m) to the top (10m) of the borehole is less than 1.5°C and consistent throughout the test. The temperature is warmest at the bottom of the borehole, and decreasing with rising depth during the test. The total test including 15h prior to test start, and 2h of recovery after test stop is covered by temperature measurements in the down flow channel. Prior to test start the top of the borehole has the coldest temperatures, with less difference in temperature between the sections at the upper half of the borehole compared to the bottom half. The temperatures at all depths are close to constant until -6h prior to test start when the temperatures is decreasing at all sections with approximate 1° before it rises again -3h prior to test start. The difference between the top and bottom of the borehole is about 3.5°. At -1.6h before test start there is a significant drop in temperature at all depths, followed by a section until test start with a temperature difference of less than 0.5°C between the top and bottom of the borehole. The section -1.5h until test has a slightly decreasing trend. At test start the temperature in the bottom of the borehole rises about 2°C, and 4-5°C in the top of the borehole.

After test stop the temperature decreases as presented in Figure 4.15 and 4.16, values of the temperature differences after different time steps are presented in Table 4.3. Immediately after test stop the temperature decreases with a larger gradient in the down flow channel, with the largest value of 1.6°C at 60m depth from the last record with heat on at the TRT rig to the first record when the heat is shut off. In general is the temperature difference decreasing with depth in the down flow channel, and increasing at the up flow. In the down flow channel is the temperature

difference greatest in the middle of the borehole at the beginning, with time is the greatest temperature differences at the sections in the upper part of the borehole. With time is also the greatest temperature difference in the up flow channel in the sections in the upper part of the borehole.

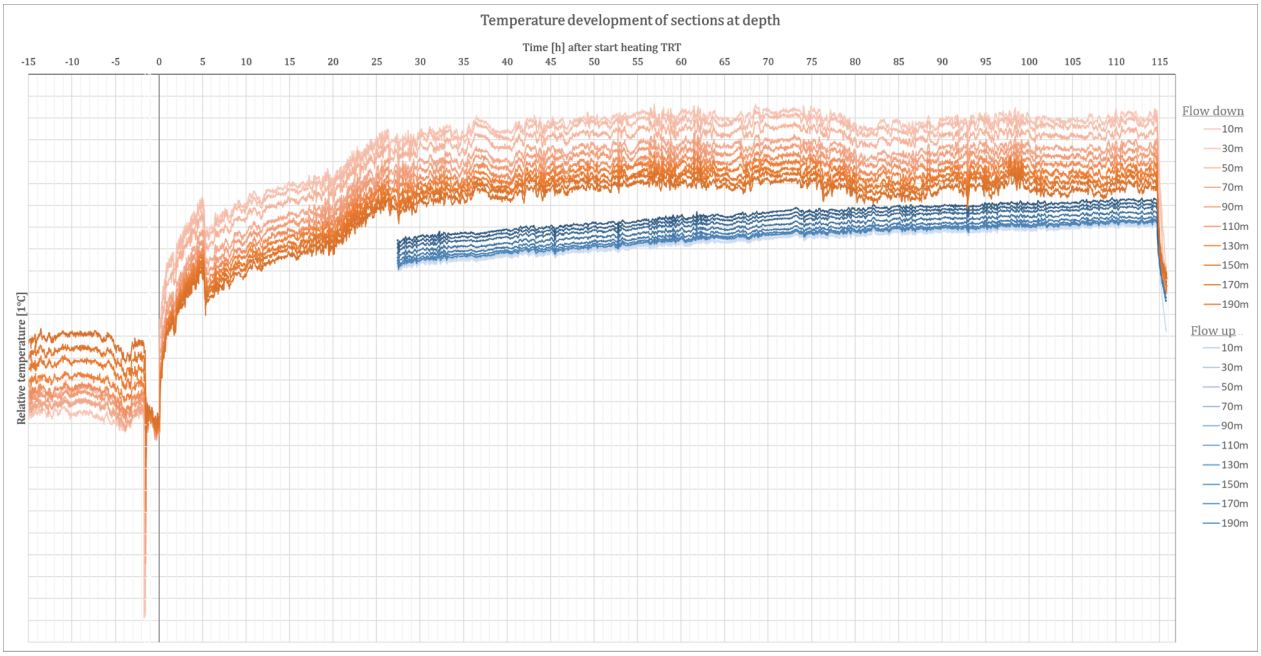

Figure 4.13: Temperature development of the collector fluid, mean values of 10m sections at depth from optical fiber measurements. The orange lines represents temperature at depths from the down flow, and blue from the up flow.

Figure 4.14: Temperature development of the collector fluid prior to and one hour after test start, presented as mean values of 10m sections at depth from optical fiber measurements in the down flow channel of the collector.

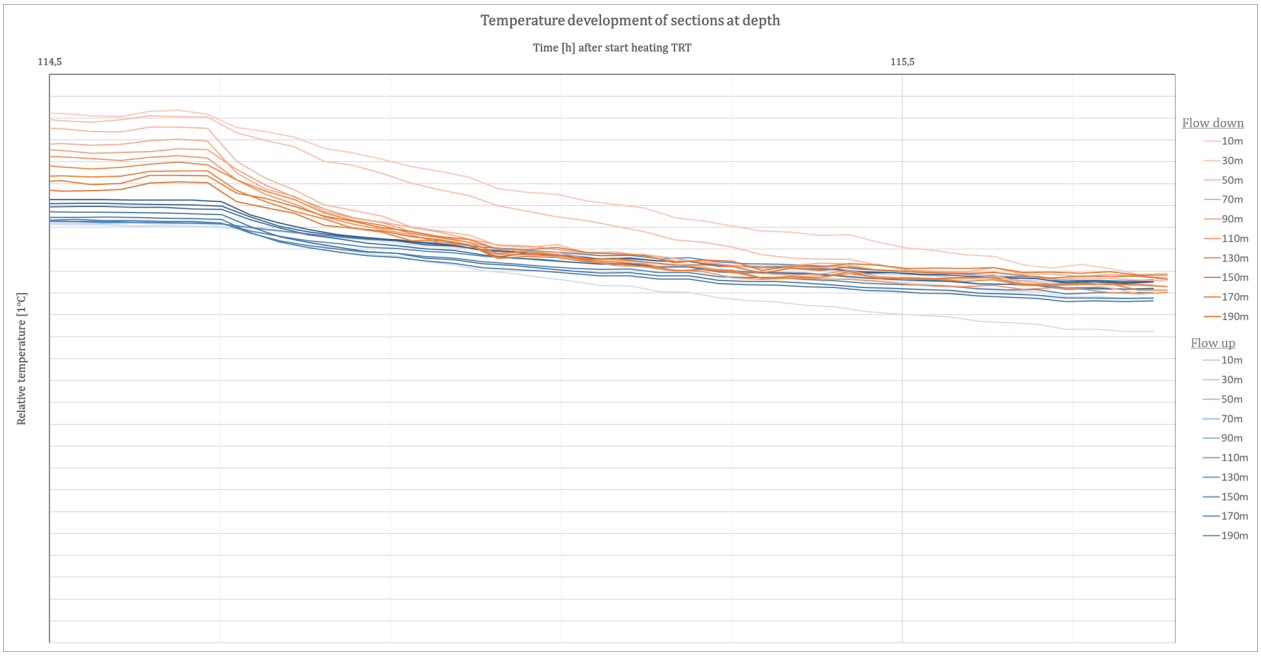

Figure 4.15: Temperature development of the collector fluid during recovery, mean values of 10m sections at depth from optical fiber measurements. The orange lines represents temperature at depths from the down flow, and blue from the up flow.

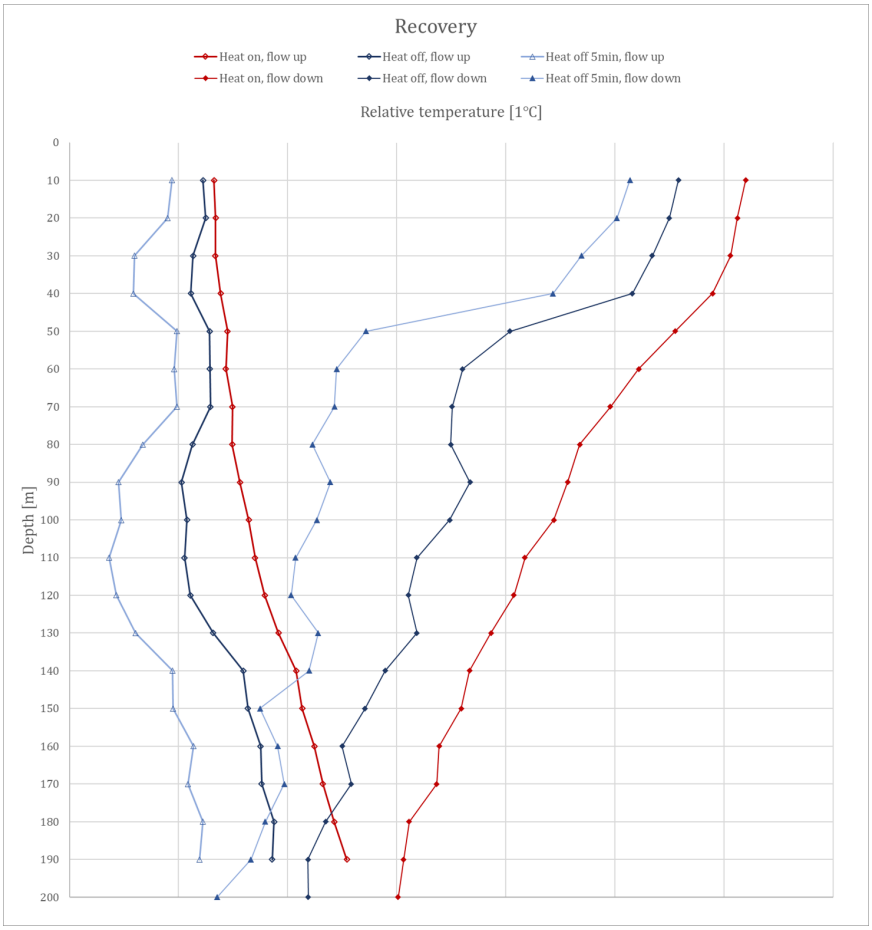

Figure 4.16: Vertical temperature profiles during recovery.

Table 4.3: Temperature differences at depth from the down flow (down) and up flow (up) records from the optical fiber after test stop for different time steps.

Depth [m]	Heat on-heat off [°C]		Heat off-5min [°C]		5-15min [°C]		15-30min [°C]		30min-1h [°C]		1-2h [°C]
	Down	Up	Down	Up	Down	Up	Down	Up	Down	Up	Down
10	-0.62	-0.10	-0.45	-0.29	-1.57	-0.55	-1.67	-0.83	-2.59	-1.43	-3.41
20	-0.62	-0.09	-0.48	-0.35	-1.94	-0.73	-1.90	-1.03	-2.44	-1.61	-2.86
30	-0.72	-0.20	-0.65	-0.54	-1.97	-1.01	-1.91	-1.23	-2.35	-1.70	-3.06
40	-0.74	-0.27	-0.73	-0.53	-2.00	-1.00	-2.01	-1.13	-2.46	-1.52	-2.58
50	-1.51	-0.17	-1.32	-0.30	-1.87	-0.50	-1.15	-0.75	-1.00	-1.03	-1.51
60	-1.61	-0.15	-1.15	-0.33	-1.74	-0.49	-1.02	-0.66	-0.90	-1.00	-1.48
70	-1.45	-0.20	-1.08	-0.31	-1.65	-0.44	-1.02	-0.68	-0.99	-1.00	-1.28
80	-1.18	-0.36	-1.27	-0.45	-1.44	-0.55	-1.04	-0.65	-1.08	-0.94	-1.29
90	-0.90	-0.54	-1.28	-0.57	-1.81	-0.56	-1.15	-0.67	-0.98	-0.92	-1.33
100	-0.96	-0.57	-1.22	-0.60	-1.72	-0.63	-1.22	-0.71	-1.04	-1.02	-1.37
110	-0.99	-0.65	-1.11	-0.69	-1.76	-0.72	-1.09	-0.73	-1.04	-0.99	-1.41
120	-0.97	-0.68	-1.07	-0.68	-1.72	-0.69	-1.16	-0.77	-1.15	-0.99	-1.36
130	-0.68	-0.60	-0.90	-0.71	-1.74	-0.78	-1.20	-0.75	-0.96	-1.01	-1.54
140	-0.77	-0.49	-0.70	-0.65	-1.79	-0.71	-0.99	-0.73	-0.98	-0.97	-1.31
150	-0.88	-0.50	-0.96	-0.69	-1.35	-0.71	-1.20	-0.76	-0.75	-1.00	-1.33
160	-0.89	-0.49	-0.59	-0.61	-1.34	-0.61	-1.02	-0.68	-0.81	-0.84	-1.24
170	-0.78	-0.56	-0.61	-0.67	-1.38	-0.65	-0.87	-0.69	-0.81	-0.90	-1.27
180	-0.77	-0.55	-0.55	-0.65	-1.34	-0.63	-0.82	-0.63	-0.72	-0.88	-1.29
190	-0.88	-0.68	-0.52	-0.67	-1.23	-0.71	-1.00	-0.72	-0.65	-0.96	-1.19
200	-0.83		-0.83		-1.27		-1.15		-0.88		-1.19

The effect (Q) and effect per meter (q) for different depth sections is presented in Table 4.4 and Figure 4.17, calculated using the temperature differences (ΔT) between sections during the TRT test inserted in Equation 3.1 together with the mean measured flow from the TRT rig during test and the material properties of the collector fluid. Except for the section at 170-180m depth is the contribution greatest at the down flow compared to the upflow. The summed contribution of the down flow is 5.98kW whereas the summed up flow contribution is 2.24kW, giving a total of 8.22kW. The mean effect of all sections are 0.46kW. There is a significant increase of the effect with the three largest values from 40m depth and the constitutive sections down, the contribution from the down flow is particular high in this range. The lowest values of the effect is present at the upper 40m of the borehole, at 80-90m, 160-170m and 180-190m depth.

Table 4.4: Calculated effect and effect per meter of depth sections.

Depth [m]	Q					q
	Down [kW]	Up [kW]	Down [%]	Up [%]	Sum	[W/m]
10-20	0.24	0.04	85	15	0.29	28.75
20-30	0.24	0.05	84	16	0.29	28.59
30-40	0.19	0.06	75	25	0.25	24.94
40-50	0.71	0.09	89	11	0.79	79.49
50-60	0.64	0.05	93	7	0.69	68.72
60-70	0.49	0.08	87	13	0.57	57.10
70-80	0.43	0.04	91	9	0.47	46.95
80-90	0.21	0.11	64	36	0.32	32.18
90-100	0.32	0.14	69	31	0.46	45.74
100-110	0.38	0.12	75	25	0.50	50.06
110-120	0.30	0.13	70	30	0.43	43.24
120-130	0.26	0.26	50	50	0.53	52.53
130-140	0.29	0.28	51	49	0.56	56.07
140-150	0.26	0.17	60	40	0.43	42.88
150-160	0.31	0.16	66	34	0.47	46.99
160-170	0.14	0.15	49	51	0.29	28.71
170-180	0.36	0.18	67	33	0.54	53.90
180-190	0.22	0.13	63	37	0.35	35.29
Sum	5.98	2.24			8.22	

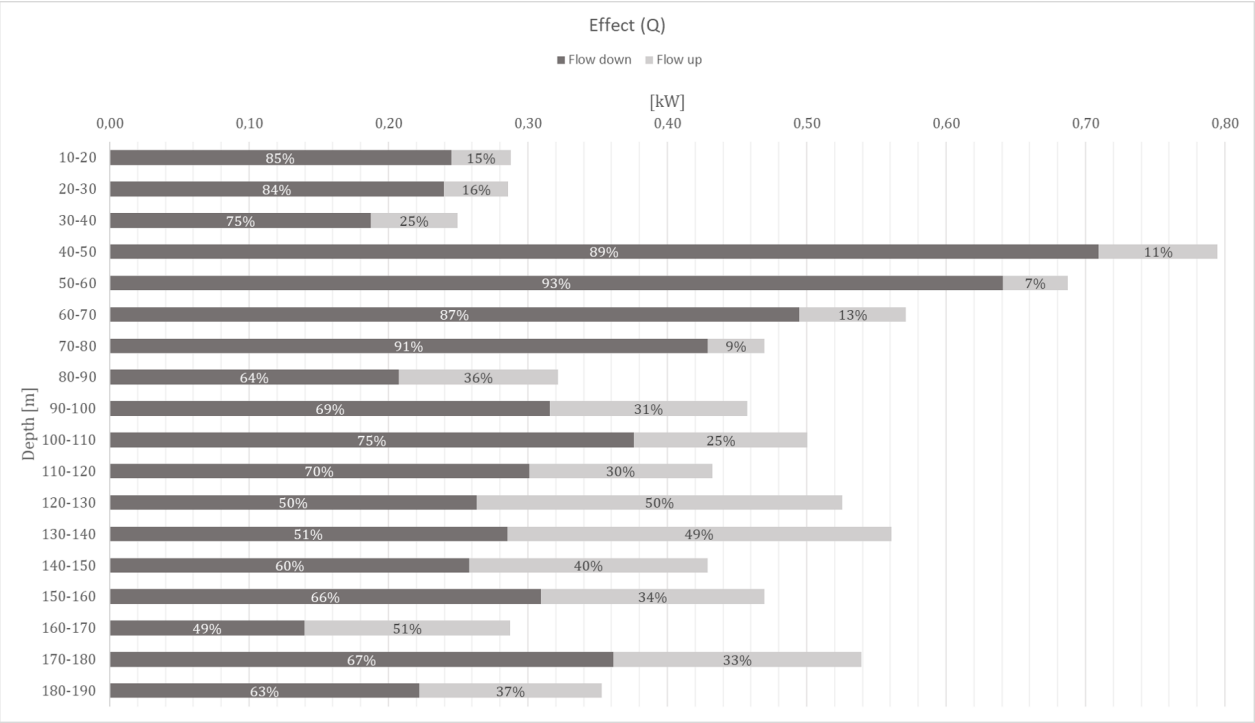

Figure 4.17: The effect (Q) at depth sections, calculated from the collector fluid flow and temperature difference between 10m sections of records from the optical fiber during the test. The percentage represents the distribution of the contributions from the down flow and up flow.

The linear regression lines fitted to the sections of temperature development with the records from the optical fiber plotted against the natural logarithm of time are given in Figure 4.18 and 4.19. The slope of the regression lines (k), together with the assigned value of effect per meter used to calculated the thermal conductivity at different depths is given in Table 4.5. The thermal conductivity of different depths is additionally presented graphically in Figure 4.20 and 4.21.

About 7.5h of data are missing for the linear regression lines from the up flow. The slope gradient for the up flow is greater (1.3-1.4) compared to the slope for the down flow measurements (0.7-0.8), both with only small variations between the sections. The ground thermal conductivity estimated from the down flow has a mean value of 3.47W/(m,K), and 0.71W/(m,K) for the estimates based on the up flow records. The ground thermal conductivity based on the up flow records have the greatest values in the lower half of the borehole, with the two most significant at 130m (1.55W/(m,K)) and 140m (1.64W/(m,K)) depth. The estimates based on the down flow records have more variation, values ranging from 1.56 to 7.75W/(m,K). The most substantial value of 7.75W/(m,K) is at 50m depth. The following sections at 60-80m, 110m, 160m and 180m depth also exceeds the mean value. The lowest values are at the upper four sections of the borehole, at 90m and 170m depth.

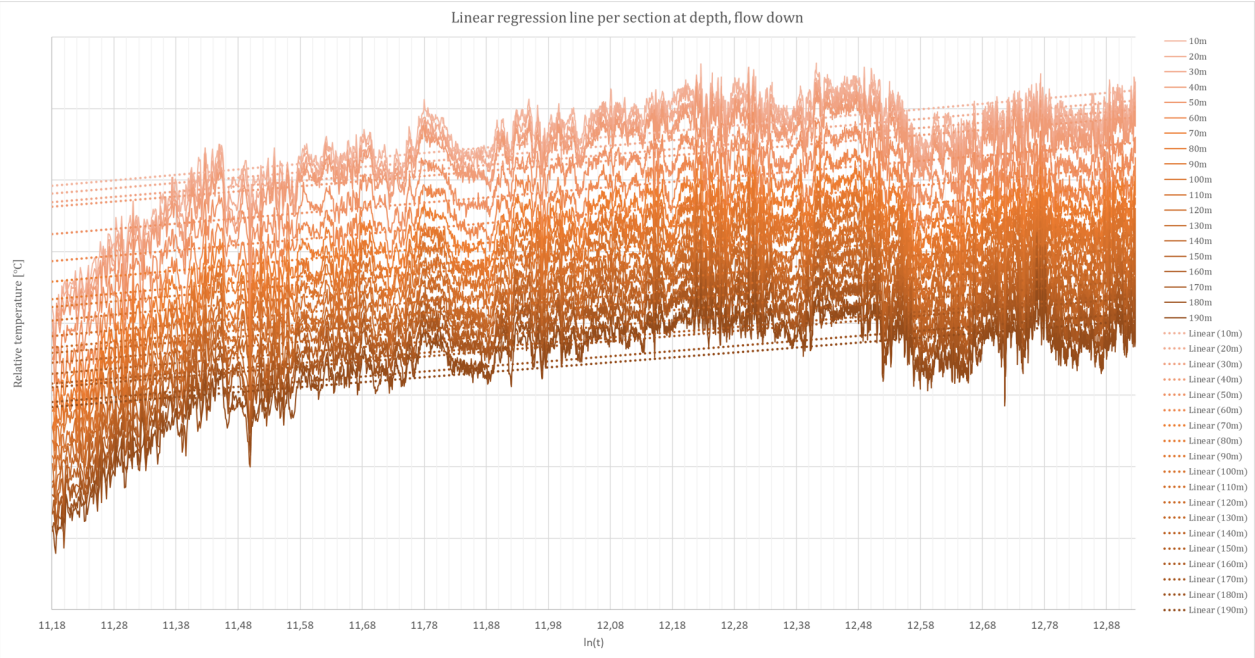

Figure 4.18: Linear regression lines fitted to the fluid temperature records from the optical fiber in the down flow channel of 10m depth sections plotted against the natural logarithm of time during TRT, excluded the first 20h of the test.

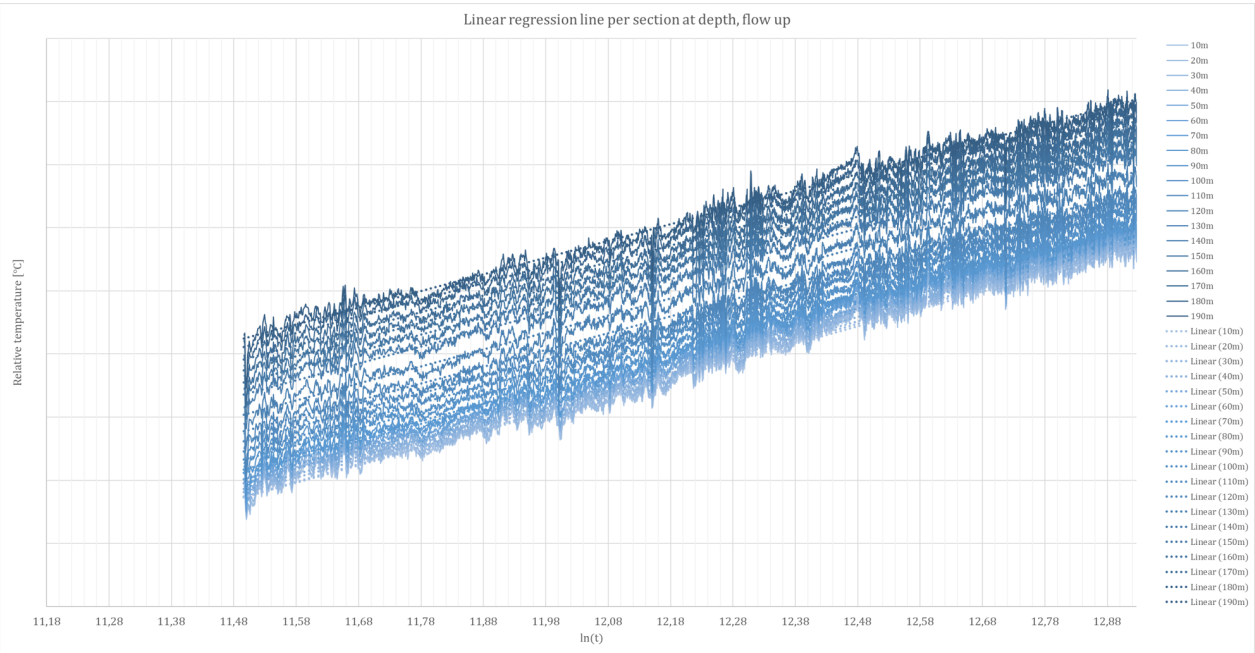

Figure 4.19: Linear regression lines fitted to the fluid temperature records from the optical fiber in the up flow channel of 10m depth sections plotted against the natural logarithm of time during TRT, data from 27.5h after test start.

Table 4.5: Estimated mean values for thermal conductivity at depth based on optical fiber records.

Depth [m]	Flow down			Flow up		
	q [W/m]	k	λ [W/(m,K)]	q [W/m]	k	λ [W/(m,K)]
10	24.49	0.76	2.55	4.26	1.38	0.25
20	24.49	0.75	2.61	4.26	1.39	0.24
30	23.98	0.74	2.57	4.60	1.38	0.27
40	18.73	0.72	2.08	6.21	1.38	0.36
50	70.92	0.73	7.75	8.57	1.39	0.49
60	64.09	0.76	6.74	4.62	1.37	0.27
70	49.46	0.77	5.09	7.64	1.36	0.45
80	42.87	0.78	4.35	4.08	1.35	0.24
90	20.75	0.79	2.10	11.44	1.34	0.68
100	31.59	0.81	3.12	14.15	1.35	0.83
110	37.60	0.81	3.70	12.45	1.34	0.74
120	30.08	0.80	3.00	13.16	1.33	0.79
130	26.34	0.75	2.81	26.20	1.34	1.55
140	28.52	0.74	3.09	27.55	1.34	1.64
150	25.80	0.75	2.75	17.08	1.33	1.02
160	30.92	0.72	3.43	16.07	1.33	0.96
170	13.97	0.71	1.56	14.74	1.32	0.89
180	36.11	0.71	4.04	17.79	1.32	1.07
190	22.22	0.69	2.57	13.07	1.32	0.79
Mean			3.47			0.71

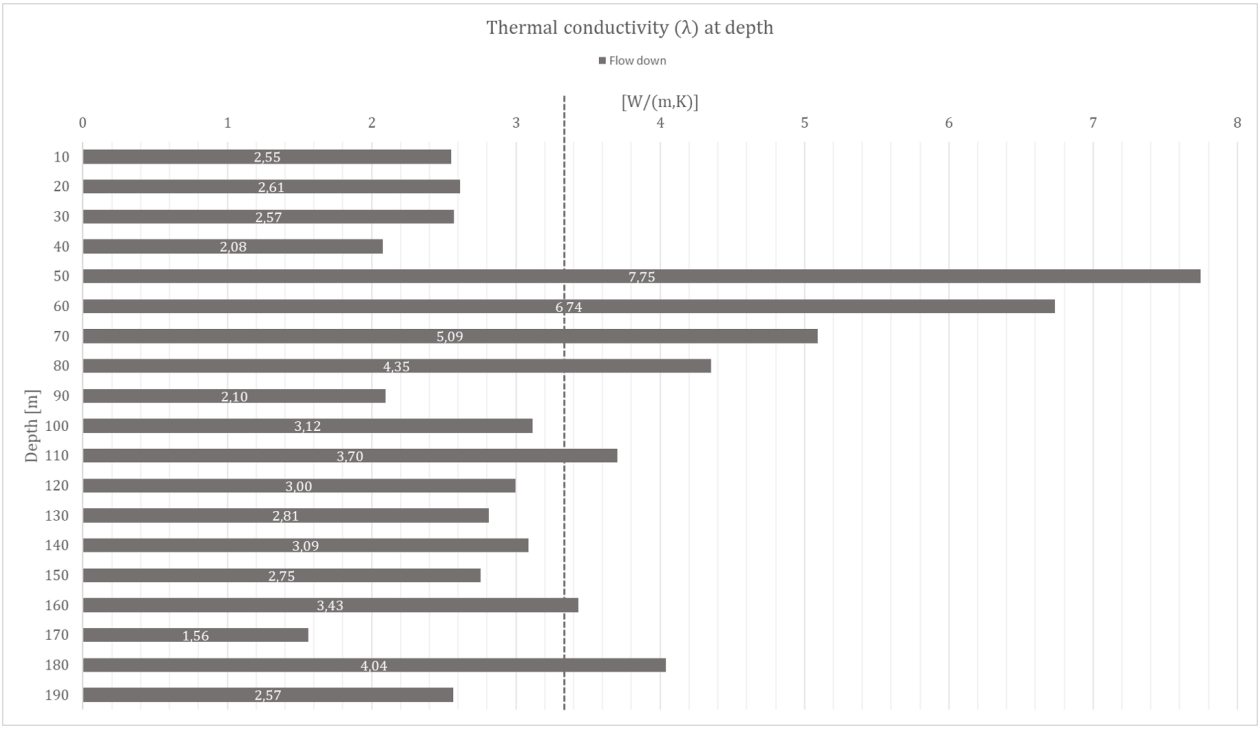

Figure 4.20: Ground thermal conductivity of depth sections calculated from the linear regression of the temperature development recorded by the optical fiber down flow, and effect per meter (q) from depth sections (Figure 4.17). The dotted line represents the average value of 3.47W/(m,K).

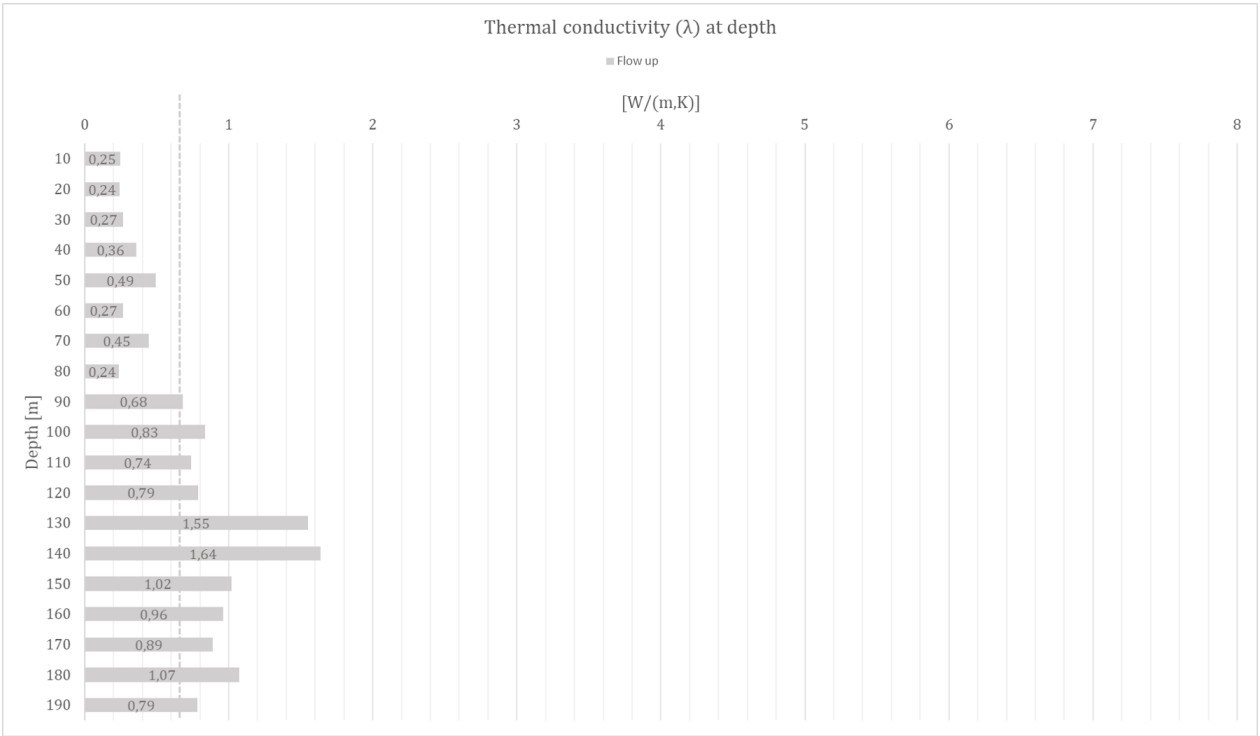

Figure 4.21: Ground thermal conductivity of depth sections calculated from the linear regression of the temperature development recorded by the optical fiber down up, and the effect per meter (q) from depth sections (Figure 4.17). The dotted line represents the average value of 0.71W/(m,K).

4.4 Numerical model

The development of temperature and 2D extent of the transient models: Transient TRT test and Transient TRT recovery are presented in Figure 4.22 and 4.23. Graphs presenting the heat rate and cumulative heat transfer passing the circumference of the borehole in the Transient TRT test model are given in Figure 4.24. The GeoStudio file containing the models are given in the Appendix, together with the reports and a movie of the temperature development during the Transient TRT test model.

After the Transient initial water analysis the 0°C isosurface has an extent radius from the center of the borehole of 50cm. Until t=3.5h, the temperature is rising both inwards and outwards from the circumference of the borehole. At t=3.5h, the temperature inside the borehole is above 9°C all following steps. The 0°C isosurface is developed to a small extent during the first steps and still has an extent radius from the center of the borehole of about 50cm at t=3.5h. The 0°C isosurface has an extent radius from the center of the borehole about 70cm after 48h and 1 at the last step (t=114.5h). The temperature is more than -1° at a radius of approximate 1.5m from the center of the borehole at the last step.

The 0°C isosurface in the Transient TRT recovery analysis is consistent with an extent radius of 1m including the time step at 48h. The extent is reduced significantly from t=72h to t=5d (120h), at t=5d the extent is approximate 25cm. At the next time step, t=5d 8h, the 0°C isosurface is at the borehole circumference. During the recovery analysis, the extent of the influenced area grows and at t=5d 8h the extent radius is about 175cm of the area over -1°C. After 15d, the temperatures at all nodes are close to the initial temperature.

The heat rate at the circumference of the borehole (Region 2) in the Transient TRT test analysis has an instant peak (0,43kW) at the first time step of the analyses. After 12h, the heat rate is reduced to 0.09kW, at the end of the test the heat rate is 0.07kW. The mean heat rate is 0.08kW. The cumulative energy transfer is 32 444kJ at the end of the analysis.

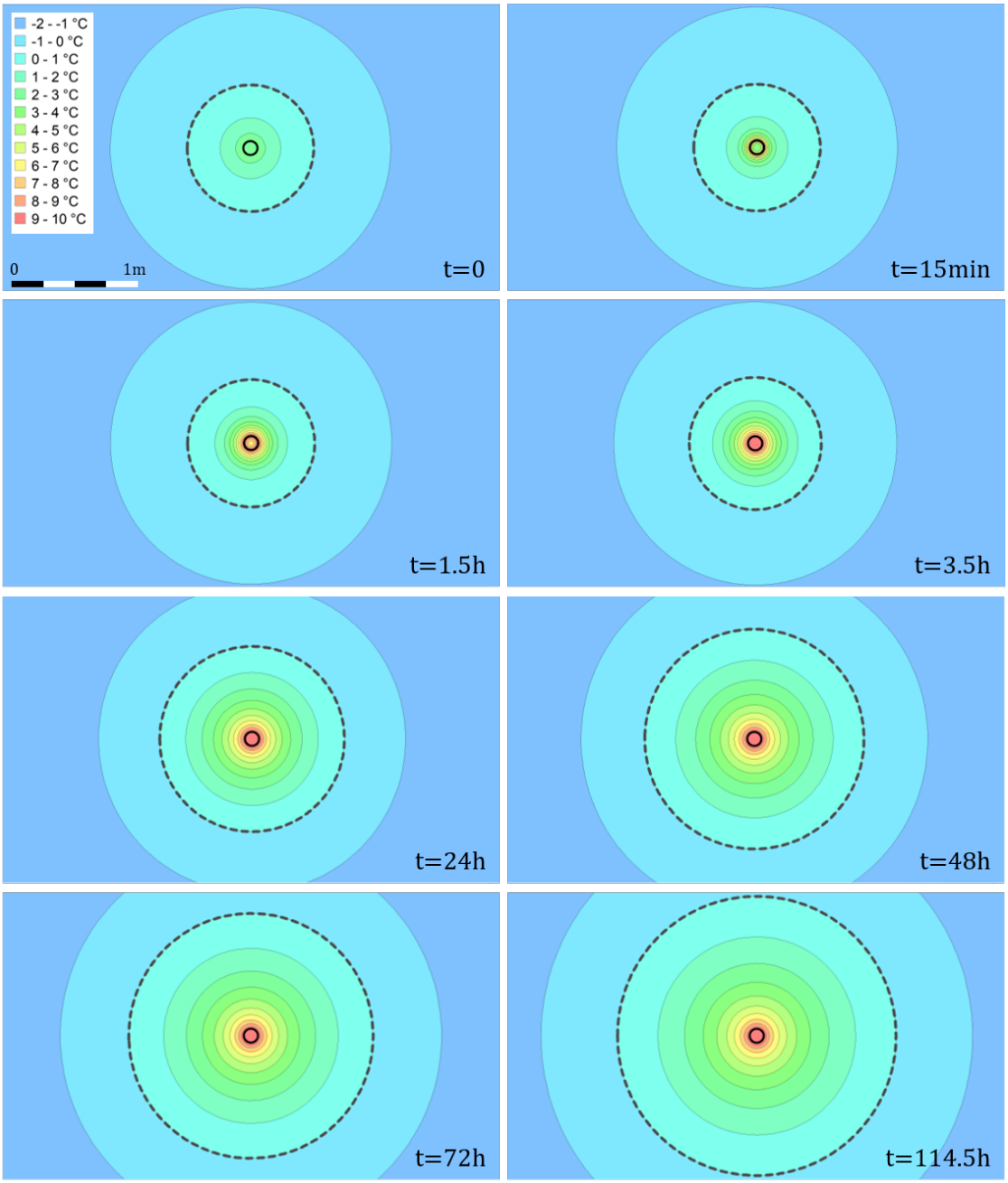

Figure 4.22: The temperature development and extent of the Transient TRT test model in GeoStudio TempW for different time steps. The upper left section (t=0) shows the initial condition of the model (the last step of the previous Transient initial water analysis), t=114.5h is the last step in the analysis. The 0°C isosurface is given by the dotted line.

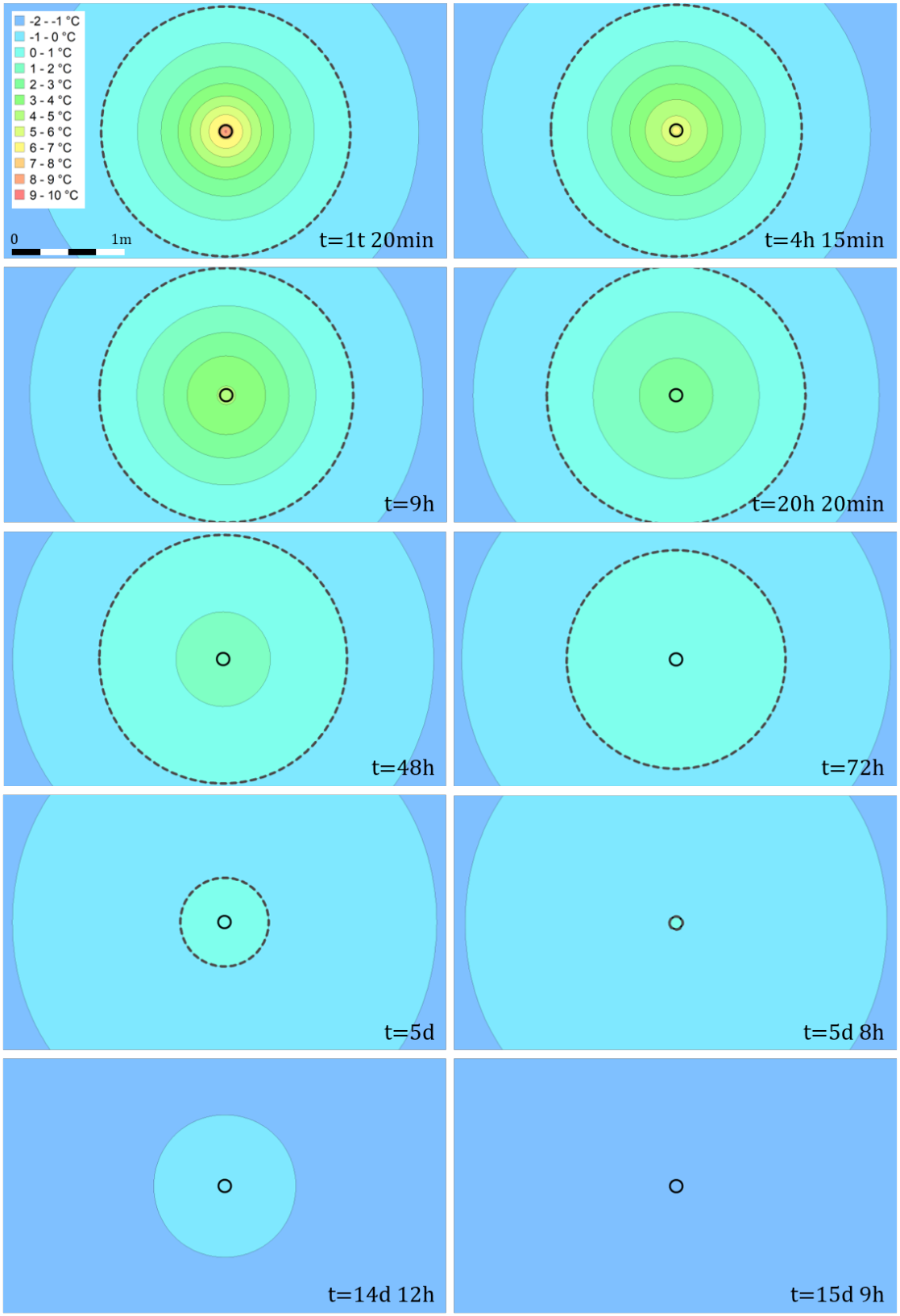

Figure 4.23: The temperature development and extent of the Transient TRT recovery model in GeoStudio TempW for different time steps (t). See t=114.5h in Figure 4.22 for initial values for the Transient TRT recovery model. The 0°C isosurface is given by the dotted line.

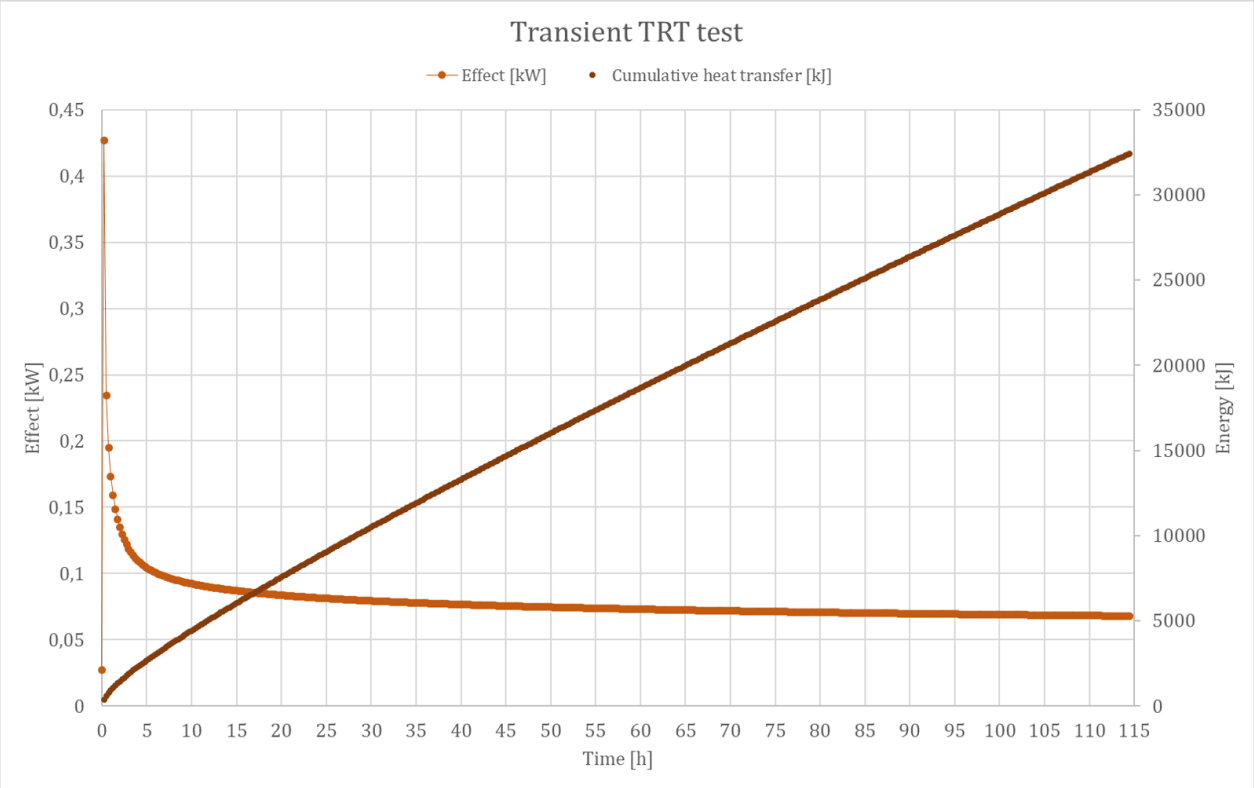

Figure 4.24: Heat rate and calculated cumulative energy transfer passing the circumference of the borehole (Region 2) during the Transient TRT test model.

5 Discussion

5.1 Drilling

Borehole B2 was successfully drilled, with a drill rate of 0.83m/min (excluding additional time for adding drill rods, etc.) and shallow depth to bedrock. There are not found a liable explanation for the source of water encountered at 8m depth, but it seems viable that the upper meters can be heavily subjected to weathering and frost actions causing water-bearing fractures. The water encountered at about 150m depth is consistent with the overpressured water-bearing sandstone found in the Helvetiafjellet Formation, and the methane is likely from the underlying Upper Jurassic Agardhfjellet or Middle Triassic Botneheia Formation (Olaussen et al. 2019). According to the drill operator the water tasted saline, and the aquifer in the Helvetiafjellet Formation is reported being brackish. The black marbling observed at the end of the drilling could be due to the reported thin coal layers in the Helvetiafjellet Formation. The observed change in colour of the dust cloud while drilling and changing drill resistance within one drill rod is in line with the reported interbedded lithology and the observed outcrop of the Carolinefjellet Formation by Veg 600.

The drilling of borehole B1 was in sediment deposits, without evidence of bedrock contact, the drilling was stopped at 57m. There was a limited amount of steel casing available, and with an overhanging danger the borehole would collapse without casing in the sediments, it was decided that the risk of loosing expensive drilling equipment was too high to continue. Sediment deposits were known present at the location, but the extent was greater than expected. The mapped surface deposits are marine shore deposits. The sediment deposits encountered at the top 15m are more evident with glaciofluvial deposits having a grain size distribution ranging from silt to gravel. The material encountered below 15m depth had a high silt and fine sand content, very dark in colour and smelly apparent evident with a high organic content. Reasonable to be in agreement with the muddy glaciomarine sedimentation in the early Holocene described by Gilbert et al. (2018).

5.2 Geological material

The collected drill cuttings samples give a representative overview and mean values of 3m depth intervals, but caution should be made regarding the results based on the drill cuttings samples as they do not represent equivalents of the bedrock types. The observations during drilling and collected drill cuttings samples are in line with already observed and reported bedrock geology in the area. The majority of the borehole is consequently within the Carolinefjellet Formation with reported immature sandstone and interbedded shale. Carbonate cementation and siderite are reported commonly for the sandstone in Carolinefjellet Formation, in agreement with the XRD results. It is assumed that the water intrusion at 150m depth marks the transition to the Helvetiafjellet Formation, which in the upper part of the formation consists of interbedded sandstone and shale with some thin coal beds. The work and database from the UNIS CO_2 Lab, including drill cores of from Dh1 and Dh2, can serve as a good source for future work including laboratory testing of the thermal conductivity of core samples.

The amorphous content of the XRD analysis may be assumed being the same material as the crystalline, but it is more likely due to weathered minerals. These are typically mica and clay minerals, resulting in these being underrepresented in the result.

5.3 Distributed Thermal Response Test

The mean values of the undisturbed ground temperature from the manual measurements had a value of -1.14°C for the total borehole, and -0.97°C from 40m depth and below. The undisturbed ground temperature found from the circulation process was -3°C. The undisturbed temperature from the circulation process at the TRT rig usually gives higher values than the manual measured temperatures due to the work done by the pump (Gehlin 2002). The difference could be due to the cold air temperature at the time, and the lack of proper isolation between the borehole and TRT rig prior to test start. The manual temperature profile measured after test stop of the TRT in borehole B2 showed a significant change in temperature at around 40m depth. This is interpreted as evidence of the groundwater level, supported by observations of the water level after drilling and the considerable change in the estimated effect at the same depth. Meaning that the water table was stabilized at about sea level. Better control of the groundwater situation with proper equipment for measuring the water table could have been performed with great advantage. In addition, water samples can be sampled during drilling in the sections with water intrusion and correlated with the work done by the UNIS CO_2 Lab for verification of the source of the groundwater. The decreasing temperature at the bottom of the profile taken after TRT test stop can be explained by ending effects at the bottom of the borehole.

The temperature measurements performed by NGU in December 2007 in boreholes Dh1 and Dh2 from the CO_2 Lab showed negative temperatures down to only 40m depth at the most, and the permafrost is reported sparse in the area by Braathen et al. (2012). Dh2 was reported drilled in November-December and the temperature measure-

ments performed in December, depending on the time from drilling activity to the temperature measurements it could be that the drilling activity have some impact on the results. This is evident with what was observed during drilling of borehole B1, having frozen material down to about 48m depth. Borehole B2 is located further up in the hillside at 40masl, and the temperature profiles imply a permafrost thickness of 160m, evident with Christiansen et al. (2010). On the contrary the temperature is high, only -1° at 15m depth, but this is probably owned to the presence of unfrozen water encountered at 8m depth when drilling.

The temperature development is most pronounced in the beginning of the test, decreasing as the temperature gradient is reduced for the approximate same added heating effect. The added heating effect and circulation flow were close to constant during the test, and using mean values for these in further calculations should therefore be acceptable. The six occasions with deviating measurements of the fluid temperature, flow, and added heating effect is coherent with the test stops to increase the pressure in the system. It can also be seen from the temperature inside the rig dropping at the same time due to the rig being opened and exposed to the outside air temperature. The significant increase in air temperature outside and inside the TRT rig is owned by an incoming storm the night after test start.

The ground thermal conductivity based on linear regression (λ_{LS}) from the conventional TRT was estimated to be 3.4W/(m,K). This agrees with the table values of sedimentary rocks from Hellström (1991). The estimated effective thermal conductivity development increases during the test. The development starting at 5h after test starts includes 15h of the early measurements compared to the development starting at 20h after test start and λ_{LS}. This consequently gives a lower ending value of 3.0W/(m,K) for the ground thermal conductivity. There are uncertainties connected to how the test responds to the presence of permafrost and how much energy went into phase change at the circumference of the borehole. This uncertainty could potentially be reduced by running a long test, pushing the boundary of the melting temperature, and then letting the borehole rest before a new test is run. The idea would be to have a second test running effecting the surrounding ground within the boundary of unfrozen ground.

The estimate of the borehole thermal resistance is closely linked to the undisturbed ground temperature. This is reflected in the estimates of the borehole thermal resistance being almost twice for the undisturbed ground temperature at -3°C (R_b=0.1(m,K)/W), compared to T_0=-0.97°C (R_b=0.06(m,K)/W). The heat transfer is most efficient in the water-filled part of the borehole, due to the thermal properties of water compared to air, this is reflected in the estimated effect at different depth sections. It therefore seems viable to estimate the borehole thermal resistance for a borehole heat exchanger in a future system from the assumption of the undisturbed ground temperature in the water-filled part of the borehole. Better estimate of the borehole thermal resistance using optical fiber cables outside the collector was not feasible due to the separate pipe for the purpose getting damaged doing installation. The borehole thermal resistance is possible to reduce by using a different set-up for the borehole heat exchanger than the simple U-pipe. On the other hand, is the simple U-pipe a cheep solution, well known and easy to install.

The distributed temperature measurements from the optical fiber records give additional information that can be used to better understand and correlate information about the geological features in the underground, and how it

affects the mean measurements from the conventional TRT. The greater difference between the top and bottom of the borehole in the down flow measurements compared to the up flow can be explained by the greater temperature gradient at the top of the borehole in the down flow, compared to the up flow flow.

The period prior to test start with close to constant temperature at different sections is a representation of the distributed undisturbed ground temperature. The very significant drop in temperature can be owned by air-cooled fluid circulating through the borehole prior to test when the system was pressurised. This is followed by the sequence of purging and circulation process. During this process, the temperature inside the collector fluid is close to constant at all depths. This period could have been used to calibrate the records from the optical fiber to the known fluid temperature measured at the TRT rig of approximate -3°. The temperature development at test start is in line with the measured mean temperatures at the TRT rig. For later use of optical fiber records would it be beneficial to make sure a section of the fiber is put in an environment with known temperature and time records that can more easily be matched during data analysis. It was not found a good way to properly calibrate the data during the analysis, and consequently the results given in relative temperature differences and axis values were removed not to confuse the reader.

After the test stop, the temperature gradient is most pronounced in the upper section of the water-filled part of the borehole in the down flow channel, and around 120-130 in the up flow channel in the beginning. This indicates areas with greater thermal conductivity. After 15min, the most significant temperature difference for both the down flow and up flow channels is in the upper part of the borehole, likely due to the air temperature influencing. The recovery period gives a valuable contribution to the understanding of the ground response after heating, unfortunately the optical fiber in the down flow was removed only 1h after the test stop, and thereafter the DTS logger stopped working 2h after test stop. For later measurements, it is recommended to extend the time period of optical fiber measurements during the recovery process.

The estimated distributed mean effect was calculated based on temperature differences between sections. As previously mentioned, the temperature differences were greatest at the down flow due to temperature gradients. The heat transfer properties of water compared to air, and the most significant increase in the estimated effect from 40m depth is evident with the assumption of the water level being at 40m depth. The summed contributions giving 8.22kW are slightly higher than the mean effect estimated from the measurement at the TRT rig of 7.8kW, which is based on the same flow and properties of the collector fluid. Some errors in the temperature difference in the optical fiber records could be from using sections with mean temperature values. Additionally, the down flow and up flow temperatures of the TRT rig were measured inside the rig and the fluid was consequently exposed to temperature contamination between the rig and borehole.

The estimated distributed mean effect per meter was further used to calculate the distributed ground thermal conductivity of different sections, based on the linear regression of the temperature development. The slope value of the linear regression lines fitted to the temperature development per section was almost twice for the up flow channel compared to the down flow, furthermore the estimated distributed effect was considerably less for the up

flow. Consequently, the distributed ground thermal conductivities based on the up flow estimates are considerably lower than the down flow estimates. As for the down flow estimates, the mean ground thermal conductivity of the sections (3.5W/(m,K)) are close to the value from the conventional analysis. The high value of thermal conductivity at the upper sections of the water-filled part of the borehole is likely due to the transition from air to water and the substantial temperature gradient in the upper part of the borehole down flow. This effect is likely reduced with depth, and the part from about 90m depth may seem to follow the same trend as the fluctuations of the quartz content in the XRD analysis. The bottom section has a lower thermal conductivity, likely due to end effects.

5.4 Numerical model

The distributed effect at 100m depth from the optical fiber measurements was estimated to be about 0.046-0.060kW, giving a cumulative heat transfer between 19-24MJ. The mean effect on the circumference of the borehole during the Transient TRT test analysis was 0.08kW, and the cumulative heat transfer 32MJ. The difference from the measured field test and the numerical model can be explained by the rough simplifications in the model: the models do not include water content in the surrounding ground (i.e. no influence of phase change), the borehole water was modelled as a solid material without convection, the boundary conditions at the borehole was set at the circumference and not as point sources inside the region - excluding the effect of borehole thermal resistance from the collector pipes and the water. Consequently, the numerical model and the extent of the radius given in the results can be treated as possible outer boundaries for how far the TRT test influences the surrounding ground.

6 Conclusion

As a contribution to the project of investigating if a High Temperature Borehole Thermal Energy Storage is feasible in Longyearbyen, the results of the pre-investigations covered in this master thesis provide encouraging results for further investigations. This includes the successful drilling of borehole B2 in the hillside at Blomsterdalen, analysis of depth-resolved temperature measurements and analysis of the mineral distribution in the encountered stratigraphy. The substantial extent of sediment deposits exceeding 57m at the location of borehole B1 makes the area not suitable for further investigations due to the expenses related to extra costs for steel casing.

Depth-resolved temperature measurements have proven to contribute to a better understanding of the underground volume tested in a Thermal Response Test. This includes the influence of the groundwater level on the heat transfer and to some extent the mineral distribution in the stratigraphy. The mean value of the estimated distributed thermal conductivity agrees with the conventional analysis of the Thermal Response Test. A reasonable value for the ground thermal conductivity is consequently 3-3.5W(m,K) in the area of borehole B2. A permafrost thickness of 160m was identified in borehole B2, some uncertainty is connected to how the phase change in the circumference of the borehole influences the results of the Thermal Response Test. Despite this, field investigations with Thermal Response Test have demonstrated to give reasonable results also in areas influenced by permafrost.

Future investigations are suggested including:

- Manual measurements of the groundwater level.
- Taking water samples during drilling to compare with known aquifers in the area.
- Keeping a section of the optical fiber in an environment with known temperature and time records for calibration.
- Extend the time for depth-resolved temperature measurements during the recovery period after test stop, and analyse the resulting temperature response.
- Include depth-resolved temperature measurements outside the collector for better estimates of the borehole thermal resistance.
- Further interpretation of the available XRD results.

References

Acuña, J. (2013). *Distributed thermal response tests: New insights on U-pipe and Coaxial heat exchangers in groundwater-filled boreholes*. Doctoral thesis. KTH Royal Institute of Technology.

Adakudlu, M., Andresen, J., Bakke, J., Beldring, S., Benestad, R., Bilt, W., Bogen, J., Borstad, C., Breili, K., Breivik, Ø., Børsheim, K., Christiansen, H., Dobler, A., Engeset, R., Frauenfelder, R., Gerland, S., Gjelten, H., Gundersen, J., Isaksen, K., Jaedicke, C., Kierulf, H., Kohler, J., Li, H., Lutz, J., Melvold, K., Mezghani, A., Nilsen, F., Nilsen, I., Nilsen, J., Pavlova, O., Ravndal, O., Risebrobakken, B., Saloranta, T., Sandven, S., Schuler, T., Simpson, M., Skogen, M., Smedsrud, L., Sund, M., Vikhamar-Schuler, D., Westermann, S. & Wong, W. (2019). *Climate in Svalbard 2100 – a knowledge base for climate adaptation.* (NCCS report 1/2019). Available at: https://www.miljodirektoratet.no/globalassets/publikasjoner/m1242/m1242.pdf (Accessed 12.04.2021.

AMAP (2017). *Snow, Water, Ice and Permafrost in the Arctic (SWIPA) 2017*. Oslo, Norway: Arctic Monitoring and Assessment Programme (AMAP).

Andersland, O. B. & Ladanyi, B. (1994). *An Introduction to Frozen Ground Engineering*. Boston, MA: Springer US. doi: 10.1007/978-1-4757-2290-1.

Austin III, W. A. (1998). *Development of an in situ system for measuring ground thermal properties*. Bachelor thesis. Oklahoma State University.

Bælum, K., Johansen, T. A., Johnsen, H., Rød, K., Ole Ruud, B. & Braathen, A. (2012). Subsurface structures of the Longyearbyen CO_2 Lab study area in Central Spitsbergen (Arctic Norway), as mapped by reflection seismic data, *Norwegian Journal of Geology*, 92(4), pp. 377-389. Available at: https://njg.geologi.no/images/NJG_articles/NJG_4_2012_2Baelum_etal_PR.pdf (Accessed: 28.04.2021).

Braathen, A., Bælum, K., Christiansen, H., Dahl, T., Eiken, O., Elvebakk, H., Hansen, F., Hanssen, T., Jochmann, M., Johansen, T., Johnsen, H., Larsen, L., Lie, T., Mertes, J., Mørk, A., Mørk, M., Nemec, W., Olaussen, S., Oye, V., Rød, K., Titlestad, G., Tveranger, J. & Vagle, K. (2012). The Longyearbyen CO_2 Lab of Svalbard, Norway - initial assessment of the geological conditions for CO_2 sequestration, *Norwegian Journal of Geology*, 92(4), pp. 353-376. Available at: https://njg.geologi.no/images/NJG_articles/NJG_4_2012_1Braathen_PR.pdf (Accessed: 28.04.2021).

Brugg Kabel AG (2017). *Fiber Optic Sensing Cables-BRUsens temperature 85°C*. Datasheet, (Rev. 05 EFR). Brugg: Brugg Kabel AG.

Carslaw, H. & J.C., J. (1959). *Conduction of Heat in Solids*. 2nd edition. Oxford: Clarendon Press.

Christiansen, H. H., Etzelmüller, B., Isaksen, K., Juliussen, H., Farbrot, H., Humlum, O., Johansson, M., Ingeman-Nielsen, T., Kristensen, L., Hjort, J., Holmlund, P., Sannel, A. B. K., Sigsgaard, C., Åkerman, H. J., Foged, N., Blikra, L. H., Pernosky, M. A. & Ødegård, R. S. (2010). The thermal state of permafrost in the nordic area during the international polar year 2007–2009, *Permafrost and Periglacial Processes*, 21(2), pp. 156-181. doi:10.1002/ppp.687.

Dallmann, W. K. (2015). *Geoscience atlas of Svalbard*. Norwegian Polar Institute.

Eklöf, C. & Gehlin, S. (1996). *TED-a mobile equipment for thermal response test: testing and evaluation*. Master thesis. Luleå University of Technology.

Gehlin, S. (2002). *Thermal response test: method development and evaluation*. Doctoral thesis. Luleå University of Technology.

Gehlin, S. (2016). 11 - Borehole thermal energy storage, in Rees, S. J. (ed.) *Advances in Ground-Source Heat Pump Systems*. Elsevier LTD, pp. 295-327. doi: 10.1016/B978-0-08-100311-4.00011-X.

Gilbert, G. L., O'Neill, H. B., Nemec, W., Thiel, C., Christiansen, H. H. & Buylaert, J.-P. (2018). Late Quaternary sedimentation and permafrost development in a Svalbard fjord-valley, Norwegian high Arctic, *Sedimentology*, vol. 65(7), pp. 2531-2558. doi:10.1111/sed.12476.

Giordano, N. & Raymond, J. (2019). Alternative and sustainable heat production for drinking water needs in a subarctic climate (Nunavik, Canada): Borehole thermal energy storage to reduce fossil fuel dependency in off-grid communities, *Applied energy*, vol. 252. doi: 10.1016/j.apenergy.2019.113463.

Gisnås, K., Etzelmüller, B., Lussana, C., Hjort, J., Sannel, A. B. K., Isaksen, K., Westermann, S., Kuhry, P., Christiansen, H. H., Frampton, A. & Åkerman, J. (2017). Permafrost Map for Norway, Sweden and Finland, *Permafrost and Periglacial Processes*, vol. 28(2), pp. 359-378. doi: 10.1002/ppp.1922.

Grimstvedt, A. & Korneliussen, A. (2000). *Bruk av XRD i kvantitative mineralbestemmelser-Eksempel Engebøf-jellet*. (NGU-rapport nr.2000.061). Trondheim: NGU. Available at: https://www.ngu.no/upload/Publikasjoner/Rapporter/2000/2000_061.pdf (Accessed: 26.02.2021).

Gustafsson, A.-M. (2010). *Thermal Response Tests - Influence of convective flow in groundwater filled borehole heat exchangers*. Doctoral thesis. Luleå University of Technology.

Hellström, G. (1991). *Ground heat storage : thermal analyses of duct storage systems*. Doctoral thesis. University of Lund.

International Permafrost Association (2021). *What is permafrost?*. Available at: https://ipa.arcticportal.org/publications/occasional-publications/what-is-permafrost (Accessed: 25.02.2021).

Isaksen, K., Førland, E., Dobler, A., Benestad, R., Haugen, J. & Mezghani, A. (2017). *Klimascenarioer for Longyearbyen-området, Svalbard*. (MET report 15/2017). Available at: https://www.met.no/publikasjoner/met-report/met-report-2017/_/attachment/download/8932a8b1-17b4-4567-8559-ed4b78d61aee:6fe02353a8212c195f00bd59dc5b2baaa6c4118c/2017-10-METreport_Statsbygg-Svalbard_final.pdf (Accessed 12.04.2021).

Kovalev, A. A., Tishchenko, L. A., Shashurin, V. D. & Galinovskii, A. L. (2017). Application of X-ray Diffraction Methods to Studying Materials, *Russian metallurgy Metally*, 2017(13), pp. 1186–1193. doi: 10.1134/S0036029517130110.

Løset, F. (2006). *Norges tunnelgeologi*. Oslo: Norges Geotekniske Institutt (NGI).

Major, H., Haremo, P., Dallmann, W., Andersen, A., Kjærnet, T. & Nøttvedt, A. (2000). *Geological map of Svalbard 1:100 000, sheet C9G Adventdalen - With map description* [map]. Norwegian Polar Institute. Available at: https://data.npolar.no/publication/7d721bdf-fa49-4ee7-a0ec-858cd807212f (Accessed 12.04.2021).

NGU (n.d.). *Geological Survey of Norway - Permafrost Svalbard Database*. Available at: http://geo.ngu.no/kart/permafrost_svalbard/ (Accessed: 16.02.2021).

Nordell, B. (1993). *Borehole heat store design optimization*. Doctoral thesis. Luleå University of Technology.

Norsk Polarinstitutt (n.d.*a*). *TopoSvalbard*. Available at: https://toposvalbard.npolar.no/ (Accessed: 14.01.2021).

Norsk Polarinstitutt (n.d.*b*). *GeoSvalbard*. Available at: https://geokart.npolar.no/geologi/GeoSvalbard/#10/78.2126/15.7632 (Accessed: 18.02.2021).

Norwegian Centre for Climate Services (n.d.). *Seklima - Observations and weather statistics*. Available at: https://seklima.met.no/observations/ (Accessed: 16.02.2021).

Olaussen, S., Senger, K., Braathen, A., Grundvåg, S.-A. & Mørk, A. (2019). You learn as long as you drill; research synthesis from the Longyearbyen CO2 Laboratory, Svalbard, Norway, *Norwegian Journal of Geology*, 99(2), pp. 157-187. doi:10.17850/njg008.

Piepjohn, K., Stange, R., Jochmann, M. & Hübner, C. (2012). *The Geology of Longyearbyen*. Longyearbyen: Longyearbyen feltbiologiske forening (LoFF).

Press release nr 003/2021 (2021). *Ny energiløsning for Longyearbyen*. Oslo: Ministry of Petroleum and Energy, Ministry of Trade, Industry and Fisheries.

Reymert, P. K. (2013). *Longyearbyen - Fra company town til moderne by*. Available at: https://www.sysselmannen.no/contentassets/bc51823074cc440f90894ba798f26a82/gamlelongyearbyen_norsk.pdf (Accessed: 08.04.2021).

Signorelli, S., Bassetti, S., Pahud, D. & Kohl, T. (2007). Numerical evaluation of thermal response tests, *Geothermics*, 36(2), pp. 141–166. doi: 10.1016/j.geothermics.2006.10.006.

Silixa (2015). *XT-DTS High Performance Ruggedised Distributed Temperature Sensor.* Datasheet. Hertfordshire: Silixa Ltd.

Skarphagen, H., Banks, D., Frengstad, B. S. & Gether, H. (2019). Design considerations for borehole thermal energy storage (BTES): A review with emphasis on convective heat transfer, *Geofluids*, vol. 2019. doi: 10.1155/2019/4961781.

Tennbakk, B., Fiksen, K., Borsche, T., Grøndahl, R., Jarstein, S., Ramm, B. et al. (2018). *Alternativer for framtidig energiforsyning på Svalbard.* (THEMA Rapport 2018-09). Available at: https://www.regjeringen.no/contentassets/cdaceb5f6b5e4fb1aa4e5e151a87859a/thema-og-multiconsult---energiforsyningen-pa-svalbard.pdf (Accessed: 12.04.2021).

Ukil, A., Braendle, H. & Krippner, P. (2012). Distributed Temperature Sensing: Review of Technology and Applications, *IEEE Sensors Journal*, vol. 12(5), pp. 885-892. doi: 10.1109/JSEN.2011.2162060.

Viseth, E. S. (2021). Vil bygge gigantisk geotermos på Svalbard, *Teknisk Ukeblad*, 24.05.2021. Available at: https://www.tu.no/artikler/vil-bygge-gigantisk-geotermos-pa-svalbard/508314?key=bogoa7rB (Accessed: 09.06.2021).

Wilke, S., Menberg, K., Steger, H. & Blum, P. (2020). Advanced thermal response tests: A review, *Renewable and Sustainable Energy Reviews*, vol. 119. doi: 10.1016/j.rser.2019.109575.

Ylvisåker, L. N. (2021). Borar etter varmelager på Svalbard, *High North News*, 15.05.2021. Available at: https://www.highnorthnews.com/nb/borar-etter-varmelager-pa-svalbard (Accessed: 09.06.2021).

Appendix

A digital zip-file containing all appendix documents can be found together with the thesis at NTNU Open. The zip-file contains the following documents:

A Field work risk assessment

B NGU Measurements

Fact sheet borehole Dh1
Fact sheet borehole Dh2

C Drill logs

Drill log registered in GRANADA - Nasjonal grunnvannsdatabase
Field observations

D XRD

E Depth-resolved temperature measurements

DTRT Down flow
DTRT Up flow
(The original raw files are kept at a NTNU database and can be accessed upon request)

F Numerical model

Reports: Steady-state initial air, Transient initial air, Transient TRT test, Transient TRT recovery
Movie Transient TRT test
GeoStudio project file including: Steady-state initial air model, Transient initial air model, Transient TRT test model, Transient TRT recovery model

NTNU
Kunnskap for en bedre verden

UNIS
The University Centre in Svalbard